HELLENIC REPUBLIC
National and Kapodistrian
University of Athens

Transferring states in quantum networks

Nikolaos Palaiodimopoulos

Ph. D Thesis

Athens 2020

This research work was supported by the Hellenic Foundation of Research and Innovation (HFRI) and the General Secretariat for Research and Technology (GSRT), under the HFRI PhD Fellowship (GA. no. 868).

Στον παππού μου

Abstract

In this work spin quantum networks are considered as a potential platform for realizing short distance quantum communication tasks. We examine the network properties that allow us to efficiently transfer quantum states between different locations. To this end we address two classes of protocols, one where the network's couplings are initially suitably engineered but remain constant throughout the transfer process and another where the couplings are time-driven. In the former case, we examine the scenario of perfect state transfer (PST) between two arbitrary nodes of the network. By studying open and closed chain geometries, we re-derive the necessary and sufficient conditions for PST and develop an analytical scheme that enables us to identify the allowed transfers. We highlight the existence of solutions where the profile of the couplings does not posses any apparent geometrical symmetry. The symmetry of the underlying network is identified by exploiting the relation between one of the necessary and sufficient conditions for PST and the recently introduced graph theoretical concept of Latent Symmetry. The presence of latently symmetric pairs of vertices is unraveled by performing an isospectral reduction. This transformation allows us to acquire the profile of the networks' couplings and therefore obtain the geometric characteristics that a network should posses in order to support PST. Furthermore, we employ the engineered couplings protocol to examine the generation of entangled states in an open chain geometry. To this end, the phenomenon of Fractional State Transfer is investigated, where we consider the transfer of a quantum state between one initial and two target sites of the network. We take steps towards obtaining the pattern of allowed and non allowed transfers and analytically obtain the necessary and sufficient conditions for this phenomenon. In addition, we prove that the bipartite nature of the chain imposes restrictions on the relative phase that appears in the generated entangled state. Finally, concerning the case where the couplings of the network are time-driven, we turn our focus on a protocol where the underlying undriven chain posses topological characteristics. Based on considerations around the nature of the adiabatic invariant and the form of the evolution of the instantaneous eigenspectrum, we propose a particular driving function for controlling the couplings, that leads to fast and robust state transfer along the chain. To prove our point, we perform a comparison with two other state transfer protocols, while to ensure robustness, we study the impact of static noise on each protocols' parameters.

Acknowledgments

First and foremost I would like to thank my supervisor Prof. F. K. Diakonos, who has accompanied me every step of the way, from my undergraduate studies till the completion of this dissertation. I consider myself extremely fortunate to have had the opportunity to learn from him, he is an excellent teacher, a wonderful person and our collaboration made me enjoy the past few years to the fullest.

My sincere thanks and gratitude goes to Prof. Dr. P. Schmelcher, whose support and collaboration was invaluable for me. Moreover, I would like to thank him for the warm hospitality when I visited ZOQ (Center for Optical Quantum Technologies) at Hamburg.

Furthermore, I would like to thank Prof. A. Karanikas (mostly for his patience) and Prof. J. Pachos for keeping an eye on my progress the past four years and for all the research directions they brought to my attention. I also want to thank the rest of members of the examination committee, Dr. D. Petrosyan, Prof. F. Mavropoulos, Prof. K. Sfetsos and Prof. N. Tetradis, their comments really helped me improve the current manuscript.

My deepest thanks to Dr. I. Brouzos, it was my pleasure working with him. Giannis has acted as a co-supervisor in this work, his physical intuition and his profound ability to break down complex problems really helped me improve my way of thinking.

Many thanks to Dr. G. Theocharis for the fruitful collaboration, it was really inspiring working with him and his vision really helped me put things into perspective.

A big thanks to my colleagues at ZOQ, Malte, Maxim and Christian for the collaboration, for their hospitality when I was there and for introducing me to the fascinating field of graph theory.

Heartfelt thanks to Eleni Holeva for helping me, more times that I can count and always with a smile.

I would also like to thank Chrysa for struggling with me, Marina for all her work and K. Zampetakis for our discussions. All the people with whom I interacted daily in the office and shared my thoughts and troubles, the younger ones: Giannis, Vaggelis and Diamantis and the previous generation: Panagiotis for supporting me all these years, Dimitris for constantly distracting me and Pantelis for sharing his wisdom.

Concluding, I would like to express my gratitude to my family and friends for their support, while special thanks goes to Eleni my advisor in life. Last but not least, I would like to thank Panagiota for helping me

revise the manuscript, prepare the presentation and for always been there for me.

Contents

1 Introduction **13**

1.1 Outline 17

2 A "static" quantum channel **19**

2.1 Preliminaries 19

2.1.1 Perfect state transfer 21

2.2 Reachability criteria 22

2.3 Network optimization 25

2.4 Open chains 26

2.4.1 6-site chain: $1 \to 4$ 27

2.4.2 7-site chain: $1 \to 5$ 27

2.5 Closed chains 30

3 Latent symmetry and PST **33**

3.1 Preliminaries 33

3.1.1 A continuous-time random walk on a graph 33

3.2 Cospectrality 34

3.3 Isospectral reduction and Latent symmetry 36

3.3.1 Latent Symmetry 37

3.3.2 4-site open chain revisited 38

3.4 What about network degeneracies? 39
3.5 Applicability 42

4 Fractional State Transfer **43**
4.1 Preliminaries 43
4.2 Reachability criteria for FST 44
4.3 Numerical results 45
4.4 Restrictions on the relative phase 48
4.5 Reachability criteria for bipartite networks 49

5 A time-driven quantum channel **51**
5.1 Preliminaries 51
5.1.1 SSH model 52
5.2 QST protocols 54
5.2.1 Topological chain 54
5.2.2 Topologically-trivial chain 55
5.3 Crucial characteristics of the driving function 56
5.4 Speed of the transfer 58
5.5 Disorder Analysis 60
5.6 Scalability 63

6 Conclusions and outlook **65**

Περίληψη **69**

Bibliography **75**

Chapter 1

Introduction

In the early 1920's the modern theory of quantum mechanics was formulated, providing us a mathematical framework for the description of nature in atomic and subatomic scales. The power of the quantum theories developed from then on, is reflected in the phenomenal accuracy of their predictions. However, since the early days of the theory, the rules constituting the mathematical foundations, yet simple, proved to be counter-intuitive. The conceptual difficulties regarding the interpretation of quantum foundations, that continue to puzzle physicists one century later on, can be seen as the harbinger of the vast challenges that one will face when trying to gain control over a quantum system.

In 1965, Moore [87] considered how the number of integrated circuit components, that are the building blocks of every electronic device, will evolve over the following years. He predicted that the number of components per integrated circuit would double once every year. The essence behind this, is that in order for the power of an electronic device to increase, the number of transistors on each component has to increase as well and consequently, the transistor's size should decrease. This implies, that the integrated components will eventually reach the scale where the quantum effects cannot be ignored and have to be treated accordingly. Letting aside the technological necessity, controlling the behavior of quantum systems, deepens our understanding of fundamental quantum processes and opens up the prospect of discovering new phenomena.

Considerations in the same spirit as described above, gradually gave rise to the field of Quantum Information. With the development of a quantum key distribution protocol [14] and the proof of the no cloning theorem [123], research on quantum cryptography was initiated. At the same time, Feynman was one of the firsts to envision a quantum computer capable of simulating physical systems [55] and a few years later Deutsch [48] was stating that, in principle, a universal quantum computer could have remarkable properties, which could not be reproduced by a classical Turing machine. This was indeed demonstrated one decade later by Grover [65] and Shor [112], who developed algorithms for solving problems in which a quantum computer could outperform its classical counterpart. At the beginning of the 20-th century, Di Vincenzo [50] summa-

rized the criteria that need to be fulfilled, in order for a device to be able to efficiently perform tasks of quantum computation and communication. In the twenty years that passed since Di Vincenzo's paper, a huge research effort has been made in order to identify and realize the most prominent platforms to this purpose.

Currently, two of the most well established platforms for realizing a quantum computer employ superconducting [49] and ion-trap qubits [74, 13]. While other ongoing directions involve neutral atoms [67, 121], semiconductor qubits [7, 108] and photons [76]. Lastly, one very appealing proposal, though until now hard to realize, employs topological protected qubits [90, 95]. In the latter approach, the topological protection, in principle, minimizes the error rate during the computation, avoiding in this way the use of error correcting codes [64], which pose a daunting challenge in all the other methods.

Existing quantum devices are able to handle a few dozens of qubits and recently quantum supremacy [104] (i.e. the ability of a quantum computer to solve a problem, whose solution is intractable in a feasible amount of time by a classical computer) was claimed to be achieved by employing a device that has the ability to handle 53 superconducting quits [3]. However, this result has been disputed [99] and there are indications that in order to realize quantum supremacy we have to gain control over at least a few hundreds qubits. Each of the aforementioned platforms has its advantages and disadvantages and in years to come it remains to be seen if one or a combination of more, will be established as the optimal implementation.

In this thesis, we will not concern ourselves with quantum computational tasks. Instead, we will focus on one of the Di Vincenzo's "desiderata" for quantum communication that was stated as follows:

"*The ability to faithfully transmit flying qubits between specified locations*"

The term "flying qubits" was used to emphasize the fact that the physical implementation of the qubits which are employed for communication tasks, will most likely differ from the ones used for quantum computation. This fact remains true even nowadays, where photons are considered to be the most reliable candidates for performing long-distance communication tasks [93]. The qubit state is usually mapped onto the polarization of the photon and can be transmitted through optical fibers. And even though proposals where electrons were considered as an alternative, have previously been made [51, 41], it wasn't until Bose's seminal work [20] that this direction flourished.

Bose proposed spin chains to act as an efficient quantum channel for short distance communication. He envisaged a circuit of quantum processors where the information can be transferred between them through spin chain quantum channels, avoiding this way the encoding of the qubit to photons. Moreover, his transfer protocol required no dynamical control over the system's parameters, therefore minimizing the errors that arise when local or global control operations take place during the transfer process. The main draw back of this approach is its scalability, since the qubit state can only be perfectly transferred along chains of very small size. To remedy this issue a new approach emerged [39, 92], where the interactions between adjacent spins are initially suitably

engineered but remain constant throughout the transfer process. In this way, Perfect State Transfer (PST) can be achieved between the two end sites of a spin chain of arbitrary length. A crucial aspect of this protocol is that the couplings between adjacent spins should follow a mirror symmetric profile (with respect to the center of the chain) in order for PST to take place. Based on the engineered coupling protocol a series of works was initiated, attempting to expand and explore its potential use. The necessary and sufficient conditions were derived [118], the quantum speed limit was deduced [126], a recursive formula for obtaining the optimal profile for the coupling strengths was proposed [120] and the effect of next to nearest neighbors [68, 78, 40] and static [46, 103, 105] or dynamical [27] disorder were considered, just to mention a few. A very comprehensive review of the subject can be found in [69, 21]. Our work was also motivated by this approach and we formulated the following research questions: Can PST occur between two arbitrary sites of the quantum channel? If not, why? If so, is there another underlying symmetry in the interactions' profile besides mirror symmetry? How are the symmetries of the interactions' profile connected with the network's geometry? To this end, we consider PST between arbitrary initial and target sites in open and closed (periodic boundary conditions) spin chains [97].

The problem of faithfully transferring a qubit state by employing a time-independent protocol, can be reduced to the problem of transferring a single excitation in a discrete network. This equivalence allowed mathematicians to treat the state transfer problem, as a continuous quantum random walk on a graph [72]. In this way, the machinery of graph theory was mobilized to tackle the problem and even though the research direction deviated from the original purpose of end to end quantum communication in a chain, more complex geometries were explored [38, 16, 11, 30, 8] and the details of the underlying dynamical evolution were treated more rigorously. In addition, another potential protocol was introduced by Godsil [61], where in order to avoid the engineering of the interactions, the PST condition is loosen up, allowing for state transfer arbitrary close to perfect, therefore named Pretty Good State Transfer (PGST). Inspired by the connection between graph theory and state transfer, we will employ the recently introduced graph theoretical concept of latent symmetry [113] and highlight its relation to the geometry of the underlying network [106], revisiting the results obtained in [97].

Another potential application of the engineered state transfer protocol is the generation of entanglement. The generation of bipartite and multipartite entanglement is of crucial importance for many quantum information tasks, ranging from quantum teleportation [15] to quantum error correction codes. Entanglement is generated by realizing the phenomenon of fractional revival in the spin chain, where the wavefunction, initially localized on one site of the chain, is found after some time perfectly splitted between the initial and the target site. Fractional revivals have been intensively studied in molecular [119] and atomic [98, 125, 6] systems and can be related to the Talbot effect [17] as well as to pattern formations of the spatial wavefunction. In [36], this direction was examined by studying the fractional revivals during the free evolution of a Gaussian wave packet in a homogeneous tight-binding model. One of the first works to consider the generation of entanglement between the two end sites of an engineered spin chain, was developed in [44]. While, an extensive study of factional revivals between the two end sites of engineered chains was been made in [58, 57]. In [71] Kay, considered fractional

revivals as a resource for state preparation and developed a numerical technique for designing the corresponding spin chains. In another recent work [10], besides studying entanglement, they employed fractional revivals to generate periodic space-time quantum interference patterns, known as quantum carpets [10]. Lastly, a series of works [31, 32, 34, 33] have addressed the problem from a graph theoretical point of view, by considering underlying networks of unweighted graphs. In this work, we will consider the fractional perfect state transfer between one initial and two arbitrary target sites of a weighted quantum chain, attempting to map the allowed transfers and identify the states that can be generated using the engineered state transfer protocol.

As stated earlier, a key feature of the engineered interaction protocol is the fact that we do not need to control the quantum channel's parameters during the transfer process. In general, depending on whether the parameters of the system vary in time or not the quantum state transfer (QST) protocols can be divided into two classes, time-dependent and time-independent respectively. Other time-independent protocols, besides the engineered chain, that have been proposed rely on Rabi-like oscillation schemes [122, 94, 59], a dual rail protocol was proposed in [25], while in [60] a transfer protocol was introduced, where local memory was used to increase the efficiency of the transfer while at the same time allowing for the transfer of multiqubit states. On the other hand, concerning time-dependent protocols, the most intuitive protocol in this case is to apply a sequence of swap operations between adjacent sites and gradually move the state along the chain. Other representative protocols were introduced in [9, 109, 26, 77].

Two of the most important factors that determine the efficiency of a QST protocol are its speed and robustness. That is, how much time it takes for the transfer to occur and how faithfully the state is transferred in the presence or absence of decoherence and static imperfections. The quantum speed limit for transferring a state along a spin chain has been studied for various protocols [47, 126, 5, 28, 128] . On the other hand, many works [46, 68, 103, 22] have examined the role of different sources of decoherence in QST protocols and proposed schemes [25, 9, 66, 1, 2] to circumvent their impact. In most cases there is a trade-off between speed and robustness, as increasing one results to the decrease of the other and vice versa.

A very promising direction towards the realization of an efficient platform able to perform fault-tolerant quantum computation comes from the field of topological states of matter [107]. One of the most appealing properties of topological systems is that they host edge states which, due to their topological protection, are robust to different sources of quantum decoherence. Recent studies [79, 114, 54, 85, 19, 82, 83], have employed 1-D topological systems, such as the Kitaev chain [75] and the SSH model [4], to act as a platform for realizing QST protocols. In this work, in the same spirit and aiming to balance the trade-off between the various factors that determine the efficiency of QST protocols, we will propose a fast and robust time-dependent protocol for transferring an excitation along an SSH chain [96].

The Hamiltonian used in all the aforementioned protocols, is quite generic and the results can be in principle applied to a variety of physical systems. The engineered J's protocol has been experimentally realized in the following setups (see Fig. 1.1). A

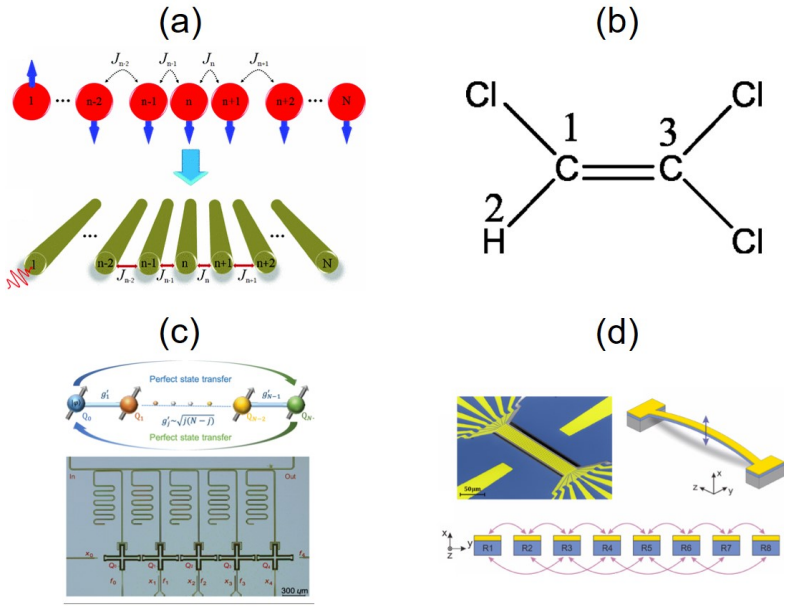

Figure 1.1: Experimental realizations of the engineered coupling protocol for perfect state transfer. (a) Array of evanescently coupled waveguides [12] (b) Liquid nuclear magnetic resonance experiment [127] (c) Superconducting transmon qubits [80] (d) Nanoelectromechanical resonators [115].

three qubit liquid nuclear magnetic resonance was used and in [127]. Experiments on an array of $N = 9$ [12] and $N = 19$ [101] evanescently coupled waveguides, were conducted as a proof of principle, while in [35] an array of $N = 11$ evanescently coupled waveguides was the first setup where high fidelity transfer was accompanied by preservation of entanglement. Moreover, in [80] the protocol was implemented in a chain of four coupled superconducting transmon qubits. Lastly, the more recent experiment was conducted in a setup consisting of $N = 8$ nanoelectromechanical resonators [115]. On the other hand, the protocols that involve time-driven couplings are much harder to realize experimentally. Nevertheless different setups ranging from, NV centers in diamond [124], superconducting circuits [116, 85], arrays of quantum dots [102], driven optical lattices [37] and NMR [29] have been proposed as potential platforms for realizing protocols with time-driven couplings. Which direction will be established as the optimal one highly depends on the feasibility of its experimental implementation.

We have tried to give a brief overview of the great efforts that have been made during the past two decades towards obtaining the optimal protocol for state transfer in quantum networks, highlighting at the same time the directions in which this work has contributed. The details of our results will be presented in the chapters to follow.

1.1 Outline

Chapter 2: We start by introducing the Heisenberg Hamiltonian and we briefly review

how spin chains can be employed to act as efficient quantum channels for transferring information in a quantum network. The concept of Perfect State Transfer (PST) together with the engineered couplings protocol are introduced. We derive the two necessary and sufficient conditions for realizing PST between two arbitrary nodes of the network (reachability criteria). We examine open and closed chains and map the reachable and non-reachable transfers. Analytically, we devise a scheme that allows us to deduce whether PST is possible or not and to extract the corresponding profiles for the couplings. Numerically, we employ an optimization algorithm based on the simplex method.

Chapter 3: We highlight the equivalency between the evolution of an excitation in an engineered quantum channel and a continuous random walk in a weighted graph. Reviewing the concept of cospectral vertices, the first reachability criterium is interpreted in terms of walks in the quantum network. We present the recently introduced concept of latent symmetry and argue that the isospectral reduction transformation can be employed to extract the symmetry profile for the sets of couplings that support PST. To demonstrate the power of this treatment we revisit some of the examples of the previous chapter. We furthermore show how the notion of strong cospectrality can handle network degeneracies connecting it with the second reachability criterium for PST.

Chapter 4: We consider fractional state transfer as a mechanism for generation of entangled states. We restrict ourselves to the case where the initial state splits between two target sites. We numerically and analytically examine open chain geometries and investigate the pattern of reachable and non-reachable target states. The reachability criteria are derived and we highlight the fact that the bipartite nature of the underlying chain imposes restrictions on the relative phase that appears on the target state.

Chapter 5: We review some basic properties of the SSH chain. We present two time-dependent QST protocols that feature almost perfect state transfer between the two end nodes of the chain when a time-driving function is imposed on the system's parameters. One where the underlying undriven channel is an odd-sized SSH chain and another where the underlying chain is topologically trivial. Based on simple considerations concerning the terms that are involved in the definition of the adiabatic invariant we identify the crucial characteristics that the driving function needs to posses, in order to speed up the transfer process for the SSH channel. We propose an intuitive function that has the aforementioned characteristics. To unravel the crucial aspects of our construction, we compare our proposal to an SSH chain possessing a different driving function, as well as, to the protocol where the underlying chain is topologically trivial. We also consider the impact of on and off-diagonal disorder ensuring the protocol's robustness and we examine its behavior as the system's size is increased.

Chapter 6: In the final chapter we conclude.

Chapter 2

A "static" quantum channel

2.1 Preliminaries

The Heisenberg Hamiltonian can be used to describe a one dimensional spin-1/2 quantum channel:

$$\mathcal{H}_{XYZ} = \frac{1}{2}\sum_{<i,j>}(J_{ij}^x\hat{\sigma}_i^x\hat{\sigma}_j^x + J_{ij}^y\hat{\sigma}_i^y\hat{\sigma}_j^y + J_{ij}^z\hat{\sigma}_i^z\hat{\sigma}_j^z) + \frac{1}{2}\sum_{i=1}^{N}B_i\hat{\sigma}_i^z \tag{2.1}$$

The chain consists of N spins, $(\hat{\sigma}_i^x, \hat{\sigma}_i^y, \hat{\sigma}_i^z)$ stand for the Pauli matrices, $(J_{ij}^x, J_{ij}^y, J_{ij}^z)$ corresponds to the strength of the exchange interaction between pairs of spins $< i, j >$ and B_i to the magnetic field. This is the so-called Heisenberg XYZ model, where XYZ characterizes the fact that the exchange interaction can be completely anisotropic. When $J^x = J^y$ we get the XXZ model and when $J^x = J^y = J^z$ the XXX model.

For the state transfer protocols we will consider in this work, unless explicitly stated otherwise, we will assume that $J^x = J^y \geq 0$, $J^z = 0$ and $B_i = 0\ \forall i$. Furthermore, we will assume that the exchange interaction is non-zero only between nearest neighbors. The Hamiltonian after these assumptions are implemented, becomes the Heisenberg XX model:

$$\mathcal{H}_{XX} = \frac{1}{2}\sum_{<i,j>}J_{ij}(\hat{\sigma}_i^x\hat{\sigma}_j^x + \hat{\sigma}_i^y\hat{\sigma}_j^y) \tag{2.2}$$

The quantum state of one spin-$1/2$ can be expanded in the basis of vectors:

$$|1\rangle = \begin{pmatrix}1\\0\end{pmatrix}, \quad |0\rangle = \begin{pmatrix}0\\1\end{pmatrix} \tag{2.3}$$

corresponding to spin up and spin down respectively, along the z-direction. Since the total spin operator $\sigma^z = \sum_{i=1}^{N}\sigma_i^z$ commutes with the Hamiltonian, every eigenstate will conserve the number of up-spins. Therefore, the Hamiltonian of Eq. 2.2 can be written in the site-basis as a block diagonal matrix, where in each block the number of up-spins

$$
\begin{array}{c}
\langle 0000| \\ \langle 1000| \\ \langle 0100| \\ \langle 0010| \\ \langle 0001| \\ \langle 1100| \\ \langle 1010| \\ \langle 1001| \\ \langle 0110| \\ \langle 0101| \\ \langle 0011| \\ \langle 0111| \\ \langle 1011| \\ \langle 1101| \\ \langle 1110| \\ \langle 1111|
\end{array}
\begin{pmatrix}
0 & 0 & 0 & 0 & 0 & 0 & 0 & 0 & 0 & 0 & 0 & 0 & 0 & 0 & 0 & 0 \\
0 & 0 & J & 0 & 0 & 0 & 0 & 0 & 0 & 0 & 0 & 0 & 0 & 0 & 0 & 0 \\
0 & J & 0 & J & 0 & 0 & 0 & 0 & 0 & 0 & 0 & 0 & 0 & 0 & 0 & 0 \\
0 & 0 & J & 0 & J & 0 & 0 & 0 & 0 & 0 & 0 & 0 & 0 & 0 & 0 & 0 \\
0 & 0 & 0 & J & 0 & 0 & 0 & 0 & 0 & 0 & 0 & 0 & 0 & 0 & 0 & 0 \\
0 & 0 & 0 & 0 & 0 & 0 & J & 0 & 0 & 0 & 0 & 0 & 0 & 0 & 0 & 0 \\
0 & 0 & 0 & 0 & 0 & J & 0 & J & J & 0 & 0 & 0 & 0 & 0 & 0 & 0 \\
0 & 0 & 0 & 0 & 0 & 0 & J & 0 & 0 & J & 0 & 0 & 0 & 0 & 0 & 0 \\
0 & 0 & 0 & 0 & 0 & 0 & J & 0 & 0 & J & 0 & 0 & 0 & 0 & 0 & 0 \\
0 & 0 & 0 & 0 & 0 & 0 & 0 & J & J & 0 & J & 0 & 0 & 0 & 0 & 0 \\
0 & 0 & 0 & 0 & 0 & 0 & 0 & 0 & 0 & J & 0 & 0 & 0 & 0 & 0 & 0 \\
0 & 0 & 0 & 0 & 0 & 0 & 0 & 0 & 0 & 0 & 0 & J & 0 & 0 & 0 & 0 \\
0 & 0 & 0 & 0 & 0 & 0 & 0 & 0 & 0 & 0 & J & 0 & J & 0 & 0 & 0 \\
0 & 0 & 0 & 0 & 0 & 0 & 0 & 0 & 0 & 0 & 0 & J & 0 & J & 0 & 0 \\
0 & 0 & 0 & 0 & 0 & 0 & 0 & 0 & 0 & 0 & 0 & 0 & J & 0 & 0 & 0 \\
0 & 0 & 0 & 0 & 0 & 0 & 0 & 0 & 0 & 0 & 0 & 0 & 0 & 0 & 0 & 0
\end{pmatrix}
$$

Figure 2.1: Matrix representation of the XX-model on the site basis, for a 4-site spin chain.

is conserved. In general, we get 2^N states of the form: $\begin{pmatrix} a_1 \\ b_1 \end{pmatrix} \otimes \begin{pmatrix} a_2 \\ b_2 \end{pmatrix} \otimes ... \otimes \begin{pmatrix} a_N \\ b_N \end{pmatrix}$, where $a_i, b_i = 0, 1$, that are separated in $N + 1$ blocks. Considering an example of a 4-site spin chain the matrix acquires the block-diagonal form depicted in Fig. 2.1.

The first to consider, a "static" QST protocol employing a spin chain quantum channel, was Bose in his seminal work [20]. To sketch Bose's idea, for convenience, we will continue considering the example of the 4-site chain. However, the analysis that follows is general. The goal is to transfer an initial state of the form:

$$\psi(t = 0) = \cos\theta \, |0000\rangle + e^{i\phi} \sin\theta \, |1000\rangle \tag{2.4}$$

from the first to the last site of the chain without applying any local or global operations during the transfer process. That means, we let the system evolve freely through the time evolution operator $\hat{U}_t = e^{-\frac{i}{\hbar}Ht}$ and after some time t^*, corresponding to the retrieval time, we expect to find the system in the target state:

$$\psi(t = t^*) = \cos\theta \, |0000\rangle + e^{i\phi} \sin\theta \, |0001\rangle \tag{2.5}$$

Due to the form of the Hamiltonian matrix we know that the action of the time evolution operator on the system eigenstates, cannot transform a state belonging to one sub-block to a state belonging to a different sub-block. Therefore, the first term of the superposition in Eq. 2.5 (corresponding to the first block of the matrix in Fig. 2.1) will "remain" as it is during the evolution (up to a phase). For the transfer to occur, we only need to ensure that:

$$e^{-i\mathcal{H}t^*} \, |1000\rangle = e^{i\xi} \, |0001\rangle \, , \tag{2.6}$$

here ξ is an overall phase and we have taken $\hbar = 1$. In this way, the problem of transferring a superposition of the form of Eq. 2.5 is reduced to the so-called one excitation

subspace of the XX Hamiltonian (see the second highlighted 4x4 block in Fig. 2.1). Therefore, from now on we will consider as our Hamiltonian the one excitation sub-block of the matrix 2.1, given by:

$$\mathcal{H} = J\sum_{k=1}^{N-1}(|k\rangle\langle k+1| + |k+1\rangle\langle k|) \tag{2.7}$$

In the last equation we have introduced the notation $|k\rangle = |0_1 0_2 ... 1_k ... 0_{N-1}\rangle$, corresponding to one spin-up excitation on the k-th site.

2.1.1 Perfect state transfer

Let us now introduce the quantity that measures how faithfully we can transfer a state between an initial $|n\rangle$ and a target $|m\rangle$ site. The quantity is called fidelity and can be given by the following equation:

$$F = \left|\langle m| e^{-i\mathcal{H}t^*} |n\rangle\right|^2 \tag{2.8}$$

which is simply the transition probability between the initial and the target site. When $F = 1$, we say that Perfect State Transfer (PST) has occured. While, the case where $n = m$, corresponds to a revival, where the wavefunction relocalizes at some time t^* on the initial site. The quantum revivals occur in every system that satisfies the prerequisites dictated by the quantum recurrence theorem [18].

In fact, the "proper" fidelity, originally introduced by Bose, is a function of the aforemention quantity and is defined as folllows:

$$\mathcal{F} = \frac{\sqrt{F}\cos\gamma}{3} + \frac{F}{6} + \frac{1}{2} \tag{2.9}$$

This definition comes from the fact that in general, the state of the n-th spin is a mixed state with a density matrix given by the following equation:

$$\rho_{out}(t) = p(t)\,|\psi_{out}(t)\rangle\langle\psi_{out}(t)| + (1-p(t))\,|0\rangle\langle 0| \tag{2.10}$$

where $p(t) = \cos^2\theta + \sin^2\theta F$ and

$$|\psi_{out}(t)\rangle = \frac{1}{\sqrt{p(t)}}(\cos\theta\,|0\rangle + e^{i\phi}\sin\theta(\langle m| e^{-iHt}|n\rangle)\,|1\rangle) \tag{2.11}$$

Equation 2.9 is obtained by integrating over all pure initial states of the n-th spin $|\psi_{in}\rangle = \cos\theta\,|0\rangle + e^{i\phi}\sin\theta\,|1\rangle$, on the Bloch sphere (i.e. $\frac{1}{4\pi}\int\langle\psi_{in}|\,\rho_{out}(t^*)\,|\psi_{in}\rangle\,d\Omega$). In Eq. 2.9, the parameter γ corresponds to the $\arg\{\langle m| e^{-iHt}|n\rangle\}$. However, this phase can be adjusted by applying an external magnetic field and thus, can be chosen to be a multiple of 2π. Consequently, since Eq. 2.9 is just a function of F, throughout this thesis when we refer to the fidelity we will consider Eq. 2.8.

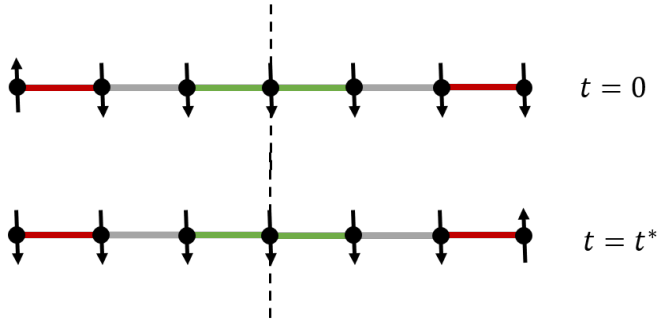

Figure 2.2: A schematic of an engineered chain with a mirror symmetric profile of the couplings (different colors correspond to different coupling strengths). (a) Initially the excitation is localized at the first site of the chain. (b) At the retrieval time t^* we find that the excitation has been perfectly transferred to the other end of the chain.

Bose examined whether PST is possible between the first and the last site of spin chains of different length and he found out that the maximum spin chain length supporting PST is $N = 4$. To remedy the lack of scalability, a modified version of the static protocol was proposed in [39, 92]. In this case, it was assumed that we are capable of suitably engineering the couplings J_i's between adjacent spins, which then remain fixed during the transfer process (see Fig. 2.2). More specifically, it was demonstrated that by enforcing a mirror symmetric profile of the form:

$$J_n = J_{N-n}, \quad n = 0, 1, ..., N-1 \tag{2.12}$$

PST could be supported between the two end sites of a spin chain of arbitrary length N. This protocol is commonly referred to as the engineered J's protocol and its main advantages are: its fastness together with the fact that no dynamical control is applied during the transfer process. The necessary and sufficient conditions for transferring a state between the two end sites ($1 \rightarrow N$) of an engineered spin chain, have been analytically determined [69, 118]. The first condition is that the couplings should follow the mirror symmetric profile that was introduced in the previous section. The second, imposes restrictions on the spectrum of the Hamiltonian.

2.2 Reachability criteria

In this section, we will analytically derive the two necessary and sufficient conditions for achieving PST by adjusting the weigths of the couplings, but without restricting ourselves to the transfer between the first and the last site of a chain. Instead we will consider the transfer between two arbitrary sites. The first to consider such a case, to our knowledge is Kay in [70]. By doing this, we aim to shed light to the underlying dynamics of the transfer process and identify the role of the network's symmetries. More specifically, we will investigate how the symmetries that appear in the coupling's profile are modified, depending on the initial and final site of the transfer. To this end, we have to note, that when examine a particular geometry, we will exclude the solutions that result in disconnecting parts of the network (i.e. $J_i \neq 0$).

We will examine two kinds of geometries, open and closed chains. By closed chains we mean that periodic boundary conditions are imposed on the system (i.e. the first site is connected to the last one). The Hamiltonian of Eq. 2.7 can be written down in matrix form:

$$\mathcal{H}_N = \begin{pmatrix} 0 & J_1 & 0 & \dots & & J_N \\ J_1 & 0 & J_2 & & & \vdots \\ 0 & J_2 & 0 & \ddots & & \\ \vdots & & \ddots & \ddots & & \\ & & & & & J_{N-1} \\ & & & & & \\ J_N & \dots & & & J_{N-1} & 0 \end{pmatrix} \tag{2.13}$$

where $J_N \neq 0$ and $J_N = 0$ correspond to closed and open chains respectively. The matrix is real and symmetric and no degeneracies are present. The case of geometries possessing spectral degeneracies will be considered in the next chapter. The eigenvalue equation writes:

$$\mathcal{H}_N \left|v_i\right\rangle = E_i \left|v_i\right\rangle \tag{2.14}$$

In order for PST to occur between the initial site $|n\rangle$ and the target site $|m\rangle$, we demand that:

$$e^{-i\mathcal{H}_N t^*} \left|n\right\rangle = e^{i\xi} \left|m\right\rangle \tag{2.15}$$

Inserting the resolution of identity $\hat{I} = \sum_{i=1}^{N} \left|v_i\right\rangle \left\langle v_i\right|$ we get:

$$\sum_{i=1}^{N} e^{i(E_i t^* - \xi)} \left\langle v_i|n\right\rangle \left|v_i\right\rangle = \sum_{i=1}^{N} \left\langle v_i|m\right\rangle \left|v_i\right\rangle \tag{2.16}$$

where $|v_i\rangle$ are linearly independent and thus, $\forall\, i$:

$$e^{i(E_i t^* - \xi)} \left\langle v_i|n\right\rangle = \left\langle v_i|m\right\rangle \tag{2.17}$$

if we add the fact that the eigenvector components of a real symmetric matrix can be chosen to be real, we end up with two equations:

$$\sin(E_i t^* - \xi) = 0 \tag{2.18a}$$

$$\cos(E_i t^* - \xi) \left\langle v_i|n\right\rangle = \left\langle v_i|m\right\rangle \tag{2.18b}$$

We consider a transfer between a set of quantum states (in our case $|n\rangle$ and $|m\rangle$) as reachable, when the states are connected through time evolution. That means, we have the ability to construct a time evolution operator that simultaneously satisfies Eq. 2.18 (a) and (b). If we assume that Eq. 2.18 (a) holds then Eq. 2.18 (b) implies that:

$$\left\langle v_i|n\right\rangle = \pm \left\langle v_i|m\right\rangle \tag{2.19}$$

which tells us that in each eigenvector of the Hamiltonian matrix the n-th and the m-th eigenvector components should be equal to each other, up to a plus or minus sign. On the other hand, Eq. 2.18 (a) gives:

$$E_i t^* - \xi = \nu_i \pi, \quad \nu_i \in \mathbb{N} \tag{2.20}$$

and taking the difference between two eigenvalues we get:

$$(E_j - E_i)t^* = (\nu_j - \nu_i)\pi \tag{2.21}$$

Without loss of generality, we can set the retrieval time to be $t^* = \pi$, which results in:

$$\frac{E_j - E_i}{E'_j - E'_i} \in \mathbb{Q} \tag{2.22}$$

This is the second reachability criterium which due to Eq. 2.22, is sometimes called the rationality criterium for the eigenvalues [38, 120].

Looking things from a slightly different perspective may actually help us gain a more intuitive picture of what the two reachability criteria stand for. The fidelity of the transfer between sites n and m is given by the following sum:

$$F = \left| \sum_{i=1}^{N} v_{in} v_{im} e^{i\phi_i} \right|^2 \tag{2.23}$$

where we have introduced the notation $v_{in} = \langle v_i | n \rangle$ and $\phi_i = E_i t$. PST dictates that the above sum should be maximized. The first reachability criterium makes a step towards this direction, by ensuring that the absolute values of the involved eigenvector components should be equal to each other $|v_{in}| = |v_{im}|$. What remains to be appropriately fixed, are the relative signs between them. Namely, the spectrum of the network should be such that there exists a time t^*, for which all the exponents $e^{i\phi_i}$ can produce an overall sign to the N terms of the sum.

In Fig. 2.3 we depict a schematic of the exponential factors $e^{i\phi_i}$ on the unit circle during a transfer process, corresponding to a system with $N = 4$. This picture is inspired by the classical analogy that was presented in [89], where the wave-packet revivals were linked to the bunching of runners on a racetrack. When $t = 0$ (see Fig. 2.3 (a)) all vectors align towards the same direction on the positive part of the real axis. For an arbitrary time $t < t^*$ (see Fig. 2.3 (b)), some vectors rotate clockwise will others anticlockwise, depending on the sign of the corresponding eigenvalue. When PST is possible, there is a time $t = t^*$ such that all vectors are aligned. In this case, all the terms in the sum of Eq. 2.23 acquire the same sign and the sum is maximized (PST). In Fig. 2.3 (c) we have singled out two cases, one where the alignment occurs on the real axis (red vectors) and another where the alignment takes place on the imaginary axis (black dashed vectors). The phases ϕ_i then, obey the following equation:

$$\phi_i = \begin{cases} n_i \pi \\ (2n_i + 1)\frac{\pi}{2} \end{cases} , n_i = 0, 1, 2, ... \tag{2.24}$$

Of course, in general, the alignment can occur in an arbitrary direction. Nevertheless, for the systems we will consider in this chapter it will become apparent that Eq. 2.24 holds. Finally, in 2.3 (d) for $t = 2t^*$ the vectors are once again aligned on the same direction (again in the general case this direction maybe arbitrary), this case corresponds to a revival where the wavefunction re-localizes on its original position acquiring a phase ξ. Note here, that this periodicity that emerges in the dynamics of a quantum system is always present when PST occurs.

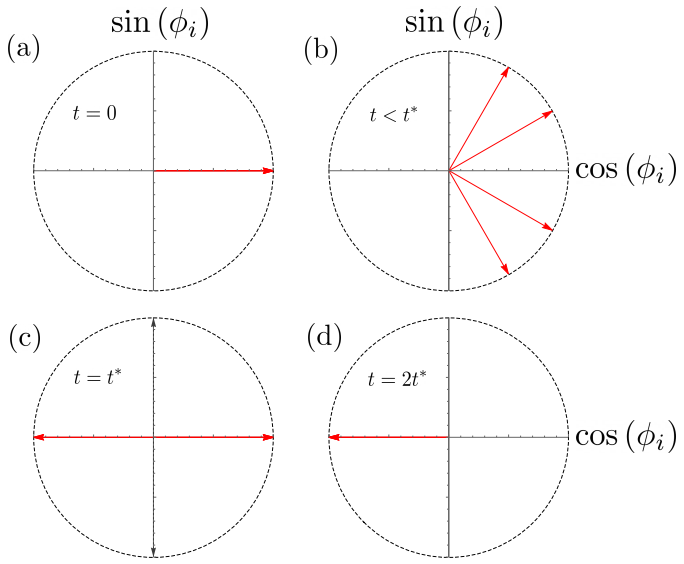

Figure 2.3: A schematic where the exponential terms of Eq. 2.23 for a system of $N = 4$, are represented as vectors on the unit circle.

2.3 Network optimization

For the open and closed geometries that will be analytically examined in the following section, the fidelity, in the absence of magnetic field, can be seen as a function of the couplings and the retrieval time:

$$F = f(J_1, J_2, ..., J_{N-1}, J_N, t^*) \tag{2.25}$$

where for open chains we have to set $J_N = 0$. Thus, for closed chains we have $N + 1$ parameters while for open chains N. Finding the set of parameters that support PST can be treated numerically as an optimization problem. Since, $F \in [0, 1]$, we can define the infidelity I, which corresponds the cost function (sometimes referred as loss function) that the optimization algorithm has to minimize.

$$I = 1 - F \tag{2.26}$$

where, in our case, the couplings and the retrieval time are the parameters with respect to which, the minimization takes place. The optimization algorithm we will use is based on the Nelder-Mead method [91]. This method is also commonly referred to as the simplex method, since it employs a polytope (i.e. simplex) of $n + 1$ vertices in the parametric space, where by n we denote the total number of parameters. After the boundaries of the parametric space are imposed, pseudo-random values are assigned on each vertex and the cost function is computed. In every step of the algorithm, different operations are applied on one or more vertices deforming the polytope. In this way the polytope scans the parametric space until a minimum is obtained, the algorithm then returns the optimal values for the set of parameters. The simplex algorithm will be our main numerical tool for deducing whether PST between a pair of vertices is possible or not. It is a reliable method for obtaining the profile of the couplings when their analytical determination becomes tedious or intractable.

2.4 Open chains

To address the second question i.e., when the reachability criteria can be met, we will now explicitly demonstrate that for certain cases the two criteria for PST cannot be met simultaneously. To do so, we first focus our study on open chains. The eigenvalue equation 2.14 is a linear system of N equations, where, each eigenvector component is defined up to an arbitrary sign s_{ij}.

$$\begin{aligned}
&J_1 s_{i2}|v_{i2}| = E_i s_{i1}|v_{i1}| \\
&J_1 s_{i1}|v_{i1}| + J_2 s_{i3}|v_{i3}| = E_i s_{i2}|v_{i2}| \\
&\vdots \\
&J_{N-2} s_{iN-2}|v_{iN-2}| + J_{N-1} s_{iN}|v_{iN}| = E_i s_{iN-1}|v_{iN-1}| \\
&J_{N-1} s_{iN-1}|v_{iN-1}| = E_i s_{iN}|v_{iN}|,
\end{aligned} \tag{2.27}$$

To deduce whether PST between the first and the m-th site is possible we will exploit the first $m-1$ equations of the linear system Eq. (2.27). By doing so, we can express $|v_{jm}|$ as a function of $|v_{j1}|$ as follows

$$|v_{im}| = \frac{E^{n-1} - E_{n\geq 3}^{n-3} \sum_{j}^{n-2} J_j^2 + E_{n\geq 5}^{n-5} \sum_{j\neq k}^{n-2} J_j^2 J_k^2 + ...}{s_{1m} \prod_{j}^{n-1} J_j} |v_{i1}|, \tag{2.28}$$

where s_{1m} is the relative sign between the first and the m-th component of v_j.Then by employing the first reachability criterium we can set $|v_{im}|/|v_{i1}| = 1$ and we end up with two energy polynomials, corresponding to the plus or minus sign of the product in the denominator. The number of the real roots of the two energy polynomials added together, has to be greater than, or equal to the total number of the system's eigenvalues otherwise PST can not be achieved.

Based on this counting argument, it is straightforward to deduce that PST from the first site to any target site $n \leq N/2$ for even-sized and $n \leq (N+1)/2$ for odd-sized chains, is forbidden. Additionally, since an open chain is mirror symmetric around the axis that passes from its center, two mirror symmetric transfer processes have the same properties. For example, when we consider the transfer from the first to the third site of a 6-site chain, based on the above, we have two second degree polynomials that can give four roots. Thus, PST cannot be made possible, since we ought to have at least six roots. By invoking the mirror symmetry of the chain, the same holds for the transfer between the fourth and the sixth site of the chain.

Moreover, specifically for odd-sized chains, because the spectrum of the Hamiltonian is symmetric, there will always be a zero energy eigenvalue. If we want to examine whether PST can occur from the n-th to the m-th site we can use Eq. (2.28) for $|v_{in}|$ and $|v_{im}|$. Using these two relations we can expunge $|v_{i1}|$ and express $|v_{im}|$ as a function of $|v_{in}|$, then by setting them equal we again end up with an energy polynomial. For the special case where m is even and n is odd or the other way around, the constant term of the polynomial is a product of the couplings. Since all the eigenvalues have to satisfy

the polynomial equation, the zero energy eigenvalue has to do so too. However, this would mean that at least one of the couplings has to be equal to zero and consequently that the chain gets disconnected. In conclusion, for odd-sized chains no PST is possible between even and odd sites.

Things get more involved when we try to rule out other PST's that do not fall into the two cases we have mentioned so far. To this purpose the second reachability criterium has to be employed. We will explicitly demonstrate an analytical scheme that can be used for these cases by considering a specific example.

2.4.1 6-site chain: $1 \to 4$

We will rule out a PST between the first and the fourth site of a 6-site chain. The energy polynomial in this case, when we set $|v_{i4}|$ equal to $|v_{i6}|$ is

$$E^3 - (J_1^2 + J_2^2)E + s_{14}J_1J_2J_3 = 0, \tag{2.29}$$

where $s_{14} = \pm 1$. By using Descartes rule we can deduce the maximum number of the polynomial's positive roots depending on the sign of the constant term. In this particular case, since we are dealing with a 6-site chain and two third degree polynomials, all the roots have to be eigenenergies of the system. For $s_{14} = +1$ the polynomial can have two real positive roots E_1, E_2 and one negative E_3. While, for $s_{14} = -1$, we get one real positive E_4 and two negative E_5, E_6. Due to the symmetry of the spectrum we also get, that $E_6 = -E_1$, $E_5 = -E_2$ and $E_3 = -E_4$. Considering the above, it is straightforward to see that the transfer amplitude becomes a sum of sines.

$$\begin{aligned}\langle 4|\, e^{-iH_6t^*}\, |1\rangle = &-2|v_{11}|^2 \sin E_1t^* - 2|v_{21}|^2 \sin E_2t^* \\ &+ 2|v_{31}|^2 \sin E_3t^*.\end{aligned} \tag{2.30}$$

Due to Eq. 2.24, we get that $\phi_i = E_it^* = (2n_i + 1)\frac{\pi}{2}$. On the other hand, employing Vieta's formula, the following equality holds for the three roots of the polynomials.

$$E_1 = -(E_2 + E_3) \tag{2.31}$$

Multiplied by t^* the above equation implies that the sum of two odd integers is an odd integer. This proves by contradiction that the two reachability criteria cannot be met simultaneously and PST is not possible for this transfer.

2.4.2 7-site chain: $1 \to 5$

Now let us consider a second example, where we examine the transfer between the first and the fifth site of a 7-site open chain. Using the linear system of Eq. 2.27, we express $|v_{i5}|$ in terms of $|v_{i1}|$. Setting them equal we obtain two energy polynomials corresponding to $s_{15} = \pm 1$.

$$E^4 - (J_1^2 + J_2^2 + J_3^2)E^2 + J_1^2J_3^2 + s_{15}J_1J_2J_3J_4 = 0 \tag{2.32}$$

For $s_{15} = +1$ we find four real roots, $\pm E_1$ and $\pm E_2$. While, for $s_{15} = -1$ a double root $E_4 = 0$ and $E_3^2 = J_1^2 + J_2^2 + J_3^2$ are obtained. Taking into account the above facts, the probability amplitude of finding the wavefunction localized at the fifth site after time t^* is given by:

$$\begin{aligned}\langle 5|\, e^{-iH_7 t^*}\, |1\rangle =& |v_{11}|^2 e^{-iE_1 t^*} + |v_{21}|^2 e^{-iE_2 t^*} - |v_{31}|^2 e^{-iE_3 t^*} \\ & - |v_{41}|^2 \\ & - |v_{51}|^2 e^{iE_3 t^*} - |v_{61}|^2 e^{iE_2^{t^*}} + |v_{71}| e^{iE_1 t^*}.\end{aligned} \tag{2.33}$$

Due to the symmetry of the energy spectrum it also holds that $|v_{11}| = |v_{71}|$, $|v_{21}| = |v_{61}|$ and $|v_{31}| = |v_{51}|$. Thus, it follows that:

$$\begin{aligned}\langle 5|\, e^{-iH_7 t^*}\, |1\rangle =& 2|v_{11}|^2 \cos E_1 t^* + 2|v_{21}|^2 \cos E_2 t^* \\ & - 2|v_{31}|^2 \cos E_3 t^* - |v_{41}|^2.\end{aligned} \tag{2.34}$$

For the amplitude to get its maximum values, an overall minus sign has to be produced from the cosines. This means, that $E_1 t^*$, $E_2 t^*$ have to be odd multiples of π, while $E_3 t^*$ even. However, from Eq. (2.32), if we multiply with t^* and employ Vieta's formula, we get

$$(E_1 t^*)^2 + (E_2 t^*)^2 = (t^*)^2 (J_1^2 + J_2^2 + J_3^2) = (E_3 t^*)^2. \tag{2.35}$$

Since, the sum of the squares of two odd integers cannot be the square of an integer, we have proved by contradiction that the transfer under consideration is not reachable.

The main point we want to highlight can be stated as follows: when the number of roots of the energy polynomials is greater than the number of the eigenvalues, the second criterium can be used in order to prove that some of these roots cannot satisfy the two reachability criteria simultaneously. It is also clear that as the length of the chain grows the number of these cases is increased, since we are forced to deal with polynomials of greater degree. We have analytically examined open chains up to 10 sites and the optimization algorithm we have used, comes in complete agreement with our analytical findings. Even though the properties of the eigenvalues of Jacobi matrices have been studied extensively [56, 117, 43], the mathematical task to prove that a number of roots of an energy polynomial of arbitrary degree cannot satisfy the rationality criterium, to our knowledge has not yet been properly addressed. As a result, there is no universal analytical procedure that can be followed to deduce whether PST between two states is possible or not. It follows that in general, each case has to be studied separately, which is something that at first sight seems discouraging. Nevertheless, the power of the analytical approach we just presented here, is that it can be applied with small modifications for each case and in order to demonstrate this fact more transparently we have considered the two previous examples.

To sum up, the following general statements can be made for open chains of arbitrary length. PST is always possible between mirror symmetric sites and this has been rigorously proven for the transfer between 1 and N [118]. In addition, transfers where both the initial and target sites are located at the first half of the chain cannot support PST. The same holds for their mirror symmetric counterparts. Finally, for odd-sized chains

we have proved that no PST is realized between even and odd sites. To these statements we will also add one that is based on our numerical results. Having examined open chains of length up to $N = 20$ sites, we have numerical evidence which support that for even-sized chains PST between the first and $N - 1$ site is always possible, in these transfers the profile of the couplings is not mirror symmetric. The rest of the cases have to be studied separately. If we are unable to prove by contradiction that PST is not supported, we have to search the parametric space and find the suitable profile for the J's that extremizes the fidelity.

This can be done numerically via an optimization algorithm or by using yet again the linear system of Eq. (2.27) to analytically extract the optimized profile for the J_i's. For the sake of illustration and to gain a more intuitive picture of the physical system under consideration, we will present an indicative example for both cases.

The first example considers the transfer from the first to the third lattice site of an open chain of length $N = 4$. This example highlights the fact that the profile of the couplings does not have to be necessarily periodic, as in the case of mirror symmetric lattice sites. In Fig. (2.4) we have plotted the probability for each of the four states on the lattice basis as a function of time, obtained by running the optimization algorithm. The system starts at the first site and then gradually the probability spreads out all over the chain, until the whole wavefunction gets localized on the third site at the retrieval time. At this

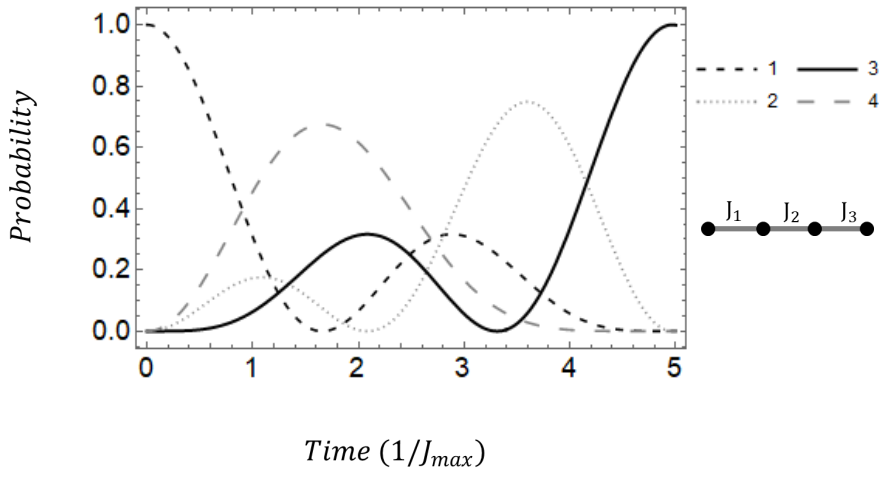

Figure 2.4: PST between sites 1 and 3. Probability for each lattice site as a function of time. Time is depicted in units of $1/J_{max}$, where J_{max} is an arbitrary unit of energy. We have set $J_1 = J_{max}$ and subsequently the optimal values for the time and the couplings are found to be $J_2 = 0.6J_{max}$, $J_3 = 0.8J_{max}$ and $t^* = 4.967/J_{max}$.

point we demonstrate that the method we suggest here to examine reachability, is also very powerful for designing the optimal profile in reachable cases. By employing the linear system of Eq. (2.27) for a 4-site chain together with the first reachability criterium we obtain the following energy polynomial

$$E^2 - J_1^2 + s_{13}J_1J_2 = 0. \tag{2.36}$$

The system has four eigenenergies that are symmetric around zero, that is $\pm E_1$ and

$\pm E_2$. It is clear that the $s_{13} = +1$ gives the pair of eigenenergies with the minimum absolute value, say $\pm E_1$, while $s_{13} = -1$ corresponds to $\pm E_2$. Having in mind the above, it is straightforward to see that

$$\langle 3| \, e^{-it^* \mathcal{H}_N} \, |1\rangle = 2|v_{11}|^2 \cos(E_1 t^*) - 2|v_{21}|^2 \cos(E_2 t^*). \tag{2.37}$$

The first pair of eigenenergies that gives an overall sign to the sum is, $E_1 t^* = \pi$ and $E_2 t^* = 2\pi$. If we multiply the equations of the linear system Eq. (2.27) with the retrieval time t^*, all quantities become dimensionless. After doing so, we can solve the linear system in terms of the couplings and time and obtain the same values as those produced by running the optimization algorithm.

2.5 Closed chains

For closed geometries, the introduction of the coupling between the first and the last site changes the system's behavior in a drastic manner. The linear system in this case takes the following form:

$$\begin{aligned} &J_1 s_{i2}|v_{i2}| + J_N s_{iN}|v_{iN}| = E_i s_{i1}|v_{i1}| \\ &J_1 s_{i1}|v_{i1}| + J_2 s_{i3}|v_{i3}| = E_i s_{i2}|v_{i2}| \\ &\vdots \\ &J_N si1|v_{i1}| + J_{N-1} s_{iN-1}|v_{iN-1}| = E_i s_{iN}|v_{iN}|. \end{aligned} \tag{2.38}$$

Let us consider PST between an arbitrary pair of sites for a closed chain of fixed length. Following the same procedure as we did for the open chains, we express the eigenvector component of the initial site as a function of the eigenvector component of the target site and we extract two energy polynomials. Due to the cyclic symmetry of the closed system, the degree of the energy polynomials is the same, independently of the choice of the initial and target sites. Namely, the highest degree polynomial for a circular chain of length N is $N-2$ for even-sized chains and $N-1$ for the odd ones.

From this perspective, it should come as no surprise that our numerical and analytical findings support the following statement: "For any closed chain of fixed length, if we can find an optimal profile for the couplings that supports PST between a particular pair of sites, then an optimal profile that supports PST between an arbitrary pair of sites always exists". Similarly, if PST is not possible for a pair of sites then the same holds for all pair of sites. Note here that we have assumed different initial and target sites. We do not take into consideration the case of quantum revivals which are always reachable.

In addition to the aforementioned facts, the even or odd length of the chain turns out to play a crucial role to the reachability of a transfer. In particular, all odd-sized chains with the exception of $N = 3$ do not support PST. On the contrary, for even-sized chains of arbitrary length, we can always obtain an optimal profile for the couplings that makes the transfer between any particular pair of states reachable.

The $N = 3$ closed chain is the only odd geometry in which PST is possible between all pair of sites. We will impose the first reachability criterium on the linear system for

the transfer between a pair of sites. Without loss of generality, we pick the first and the third site. Then, depending on which equations we use, we can either obtain a second degree polynomial

$$E^2 - s_{13}J_3E - J_1(J_1 + s_{13}J_2) = 0, \tag{2.39}$$

or a first degree polynomial

$$(J_2 - s_{13}J_1)E + J_3(J_1 - s_{13}) = 0. \tag{2.40}$$

In Eq. (2.39), we expect that one choice of the sign s_{13} will give one eigenvalue, while the other choice, will give the other two eigenvalues. On the other hand, by observing Eq. (2.40) we could immediately state that, since two first degree polynomials cannot give three solutions, PST is not possible. This however is not the case here. For $s_{13} = -1$ we get that $E_1 = -J_3$ but for $s_{13} = +1$ we can pick $J_1 = J_2$ which gives an infinite number of solutions and thus we can avoid the contradiction. In conclusion, PST is realized in this system as long as $E_1 = -J_3$ and $J_1 = J_2$. The $N = 3$ closed geometry is the only case where a specific choice of the couplings can lead to an omission of the highest order term in the energy polynomial. For all the other odd closed chains ($N > 3$), PST is not supported. To analytically demonstrate this fact, we can demand that the energy polynomials, obtained from the linear system (2.38), possess as roots the system's eigenvalues, arriving this way to a contradiction. For the even-sized closed chains, the optimal profile for the couplings that supports PST between a particular pair of states, can be obtained by the same scheme that was developed in the previous section.

Nonetheless, the optimization algorithm, as the system's length grows, remains our strongest tool for obtaining the optimal profile for the couplings. Thus, it is worth highlighting a property, that besides its physical importance, enables us to make the optimization algorithm more efficient. When running the algorithm we obtain many solutions for the coupling's profile in reachable cases. Of particular importance is the fact that, there always exists a solution which is locally symmetric on the two different "paths" (clockwise, anti-clockwise) leading from the initial to the target site. To clarify further this point, we will consider a specific example.

In Fig. (2.5) we show the probability for each lattice site for an engineered profile of the couplings, that supports PST between the first and the third site of a 6-site closed chain. By observing the values of the couplings we can easily notice that, for the path that goes clockwise from the first to the third lattice site, $J_1 = J_2$. For the anti-clockwise path, the profile is again parity symmetric ($J_3 = J_6$ and $J_4 = J_5$). Therefore, by imposing such symmetries on the couplings, we can drastically reduce the dimensions of the parametric space in which the optimization algorithm searches for solutions. In the following chapter we will investigate the root of the emerging symmetries on the profile of the couplings for a quantum network of arbitrary geometry.

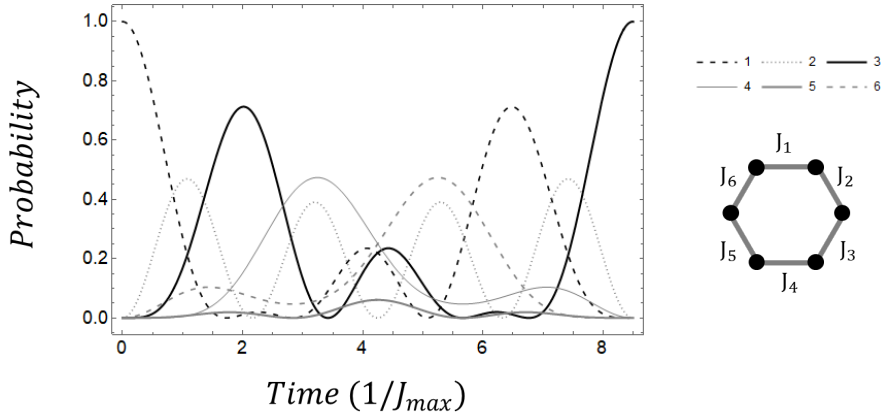

Figure 2.5: PST between site 1 and 3. Probability for each lattice site as a function of time. Time is depicted in units of $1/J_{max}$. We have set $J_1 = J_{max}$ and subsequently the optimal values for the time and the couplings are found to be $J_2 = J_{max}$, $J_3 = J_6 = 0.369J_{max}$, $J_4 = J_5 = 0.547J_{max}$ and $t = 8.494/J_{max}$.

Chapter 3

Latent symmetry and PST

3.1 Preliminaries

In this chapter we will identify the graph theoretical concepts related to the phenomenon of PST in discrete networks and unravel the underlying geometrical symmetry that has to be imposed between two sites in order to be able to support PST. Our aim is twofold, on the one hand we want to highlight the power of the tools developed in graph theory, most of which remain blurry in the physics community. On the other, we will demonstrate how these concepts will allow us to gain a deeper understanding of the underlying dynamics of the PST process and indicate in which ways we can employ them in order to extend our means of controlling and designing quantum networks that feature PST.

3.1.1 A continuous-time random walk on a graph

A graph $G(V, E)$ denotes a set of objects, commonly addressed to as vertices V, pairs of which are connected. We will consider weighted graphs, where their connections belonging to the set E are called edges and each element e_{ij} (connecting vertices i and j) is weighted by a function $w : E \to \mathbb{R}^+$. A graph G can be fully specified by its adjacency matrix A_G which is defined as follows:

$$A_G = \begin{cases} w(i,j) & \text{for} \quad e_{ij} \in E \\ 0 & \text{otherwise} \end{cases} \tag{3.1}$$

When all the edges have the same value, the graph is called unweighted and the value 1 is used to signify the existence of an edge. In the case of a weighted graph, arbitrary values can be assigned to every edge, we will restrict ourselves to positive real numbers. In Fig. 3.1, we give a diagrammatic representation of a weighted graph G_1 consisting of 3 vertices and 4 edges together with its adjacency matrix A_{G_1}. Note, that the diagonal entries in the adjacency matrix correspond to edges that are connecting the vertices to themselves and are diagrammatically represented by loops. Let $\psi(t)$ be a

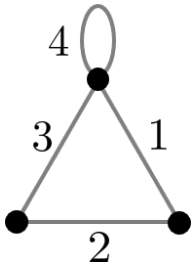

$$\begin{pmatrix} 4 & 1 & 3 \\ 1 & 0 & 2 \\ 3 & 2 & 0 \end{pmatrix}$$

Figure 3.1: A weigthed graph consisting of 3 vertices and 4 edges, together with its adjacency matrix.

time dependent-vector on the vertices of G, then for a continuous-time quantum random walk starting from the vertex a the evolution is given by

$$|\psi(t)\rangle = e^{-itA_G} |a\rangle \tag{3.2}$$

where $|a\rangle$ corresponds to a unit vector of the form $|00...1_a...0\rangle$, defined in the basis of the adjacency matrix. The adjacency matrix of a graph has an one to one correspondence with the Hamiltonian matrices we considered in the previous chapter. The vertices correspond to sites, the weighted edges to the couplings between the spins and the weighted self-loops to the magnetic field on each site. Thus, from now on we may use the aforementioned terms interchangeably. We say that PST occurs between vertices a and b when:

$$\left|\langle b| e^{-it^* A_G} |a\rangle\right| = 1 \tag{3.3}$$

where t^* corresponds to the retrieval time.

3.2 Cospectrality

In the previous chapter we have introduced two reachability criteria which pose the necessary and sufficient conditions for PST. The first reachability criterium for two vertices a and b, belonging to a graph G of N vertices, writes:

$$|\langle v_i|a\rangle| = |\langle v_i|b\rangle| \quad i = 1, 2, ..., N \tag{3.4}$$

where v_i corresponds to the i-th eigenvector of the Hamiltonian matrix.

When Eq. 3.4 holds the vertices a and b are said to be cospectral [110]. Cospectrality is a property that has been related to PST [63] and the following statements are equivalent [63]:

1. vertices a and b are cospectral
2. $\sigma(H \setminus a) = \sigma(H \setminus b)$
3. $(H^k)_{a,a} = (H^k)_{b,b}\ \forall k$

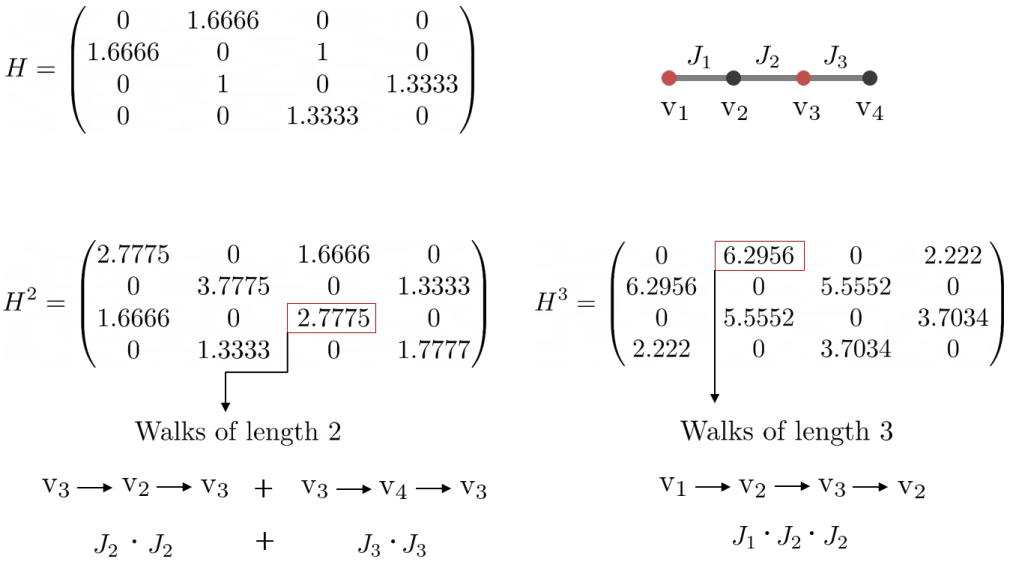

Figure 3.2: The first three powers of a 4-site open chain supporting PST between vertices v_1 and v_3. For the highlighted elements of H^2 and H^3, we demonstrate how the entries of each matrix can be interpreted in terms of walks.

By $\sigma(H \setminus a)$ we denote the spectrum of the Hamiltonian matrix computed after the row and column corresponding to the vertex a, have been deleted. Of particular importance is the third equivalent definition of cospectrality, since it allows us to interpret the concept in terms of walks in the graph. We will demonstrate this geometrical picture of the matrix powers of the Hamiltonian by considering a simple example that was examined in Chapter 2. Namely, we will consider a 4-site chain supporting PST between the first and the third vertices. We have previously raised the importance of this example, that belongs to the class of transfers where the profile of the couplings is not mirror symmetric. In Fig. 3.2 we have computed the first 3 matrix powers of the Hamiltonian for a set of couplings that supports PST between v_1 and v_2. We will now proceed and give the interpretation of the matrix entries in terms of walks. For an entry $(H^k)_{i,j}$, the matrix power k corresponds to the number of steps we can take, while the subscripts i, j correspond to the initial and final vertices of the walk. For the calculation of each entry, what we basically do is adding all the possible walks of length k between the i-th and the j-th vertices, while at the same time compensating for the weights of the edges. Taking for example $(H^2)_{3,3}$ we have two options for realizing a walk of length 2 starting and ending at the third vertex. The first is to go, $3 \to 2 \to 3$ and the other is $3 \to 4 \to 3$, each time an edge is crossed we have to multiply with the corresponding weight and at the end the walks have to be added together. Therefore, for this particular example, we get $(H^2)_{3,3} = 1 \cdot 1 + 1.3333 \cdot 1.3333 = 2.77769$. Following the same procedure, all the matrix entries of each power of the Hamiltonian matrix can be computed. In Fig. 3.2, we provide an additional example by considering the off-diagonal entry $(H^3)_{1,2}$.

Based on the above discussion, we can relate the first reachability criterium with the geometry of the network, restating it in the following way: One of the necessary conditions a quantum network should satisfy in order for PST to occur between vertices a and b, is that the sum of all the weighted walks of length k starting and ending on

vertex a should be equal to the corresponding sum of walks of vertex b (i.e. $(H^k)_{a,a} = (H^k)_{b,b}$) and this should hold for every power of the Hamiltonian matrix. Actually here, by taking advantage of the Caley-Hamilton theorem, which states that a square matrix satisfies its own characteristic equation, for a Hamiltonian consisting of N vertices, it directly follows, that it suffices to ensure that this holds for all $k \leq N-1$.

3.3 Isospectral reduction and Latent symmetry

We will now briefly review another concept originating from network theory, that goes by the name isospectral reduction [24]. The purpose of the isospectral reduction transformation, as the name suggests, is to reduce the dimension of a matrix H in $\mathbb{C}^{N\times N}$, while at the same time preserve its spectral information. In order, for a smaller matrix to be able to preserve the eigenvalues of the original matrix, rational functions are employed. The isospectral reduction is performed over a set of vertices S and is defined in the following way:

$$R_S(H,\lambda) = H_{SS} - H_{S\bar{S}}(H_{\bar{S}\bar{S}} - I\lambda)^{-1}H_{\bar{S}S} \tag{3.5}$$

by $\bar{S}$ we denote the complement of S, that is the rest of the vertices that are not included in the set S. The matrices H_{SS} and $H_{\bar{S}\bar{S}}$ are obtained by deleting all the vertices of $\bar{S}$ and S respectively, while $H_{S\bar{S}}$ and $H_{\bar{S}S}$ correspond to the connections between set S and $\bar{S}$. The isospectral reduction is defined for all values of λ besides the ones that correspond to eigenvalues of $H_{\bar{S}\bar{S}}$, we will denote this set by $\mathcal{L}$. Thus, the isospectral reduction is properly defined when $\lambda \in \mathcal{L}$. The eigenvalues of the reduced matrix $R_S(H,\lambda)$ are given by:

$$det(R_S(H,\lambda) - \lambda I) = 0 \tag{3.6}$$

If the spectrum of $H_{\bar{S}\bar{S}}$ does not contain any eigenvalues of the original matrix H then all the eigenvalues of H are given by Eq. 3.6. On the contrary, the eigenvalues of H that are contained in the spectrum of $H_{\bar{S}\bar{S}}$ are excluded from the spectrum of $R_S(H,\lambda)$. Thus, for the spectrum of the reduced matrix $\sigma(R_S(H,\lambda))$ we get:

$$\sigma(R_S(H,\lambda)) = \sigma(H) - \sigma(H_{\bar{S}\bar{S}}) \tag{3.7}$$

In Fig. 3.5 we give two representative examples, one where the initial graph is reduced over three vertices and all spectral information is preserved and one where the reduction over two sites does not contain all the eigenvalues of the initial graph.

We have to highlight here an important aspect of the reduction that will be proved to be crucial for our approach. The reduced matrix obeys the eigenvalue equation:

$$R_S(H,\lambda_i)\tilde{\mathbf{v}}_i = \tilde{\lambda}_i\tilde{\mathbf{v}}_i \tag{3.8}$$

where by $\tilde{\lambda}_i$ and $\tilde{\mathbf{v}}_i$ we have denoted the eigenvalues and eigenvectors of $R_S(H,\lambda_i)$. Note, that the eigenvectors $\tilde{\mathbf{v}}_i$ do not have to form an orthogonal basis and in principle,

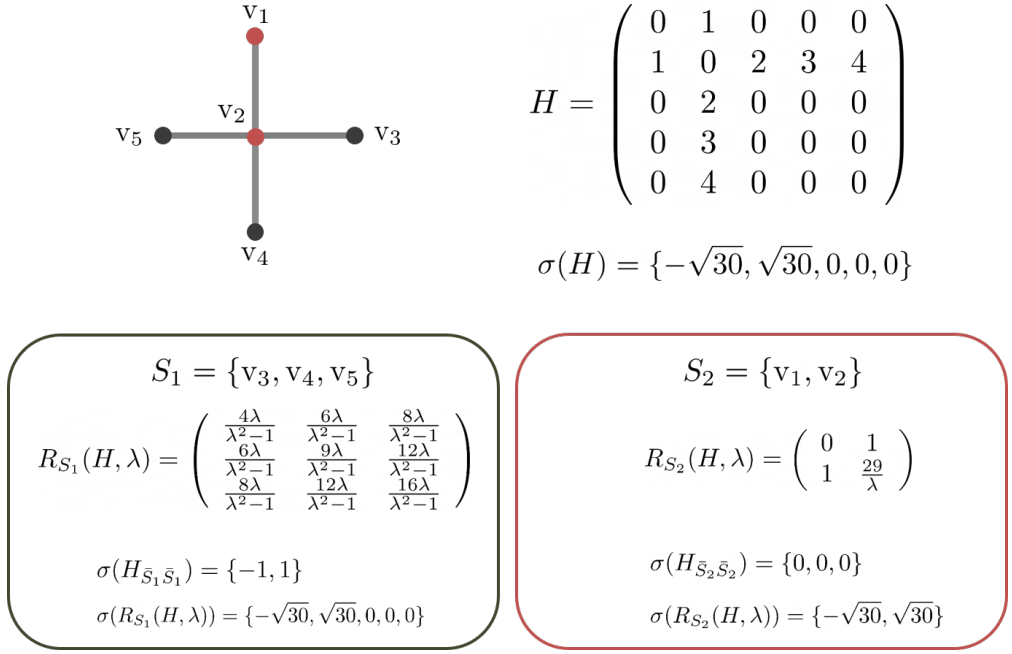

Figure 3.3: A 5-vertex graph is given together with its Hamiltonian matrix H and its spectrum $\sigma(H)$. In the first case (bottom left) the reduction is performed over the set $S_1 = \{v_3, v_4, v_5\}$, while in the other (bottom right), over $S_2 = \{v_1, v_2\}$. For both cases, we provide the spectrum of the reduced matrix together with the spectrum of $H_{\bar{S}\bar{S}}$.

could even be linearly dependent or pairwise identical. However, they are related to the eigenvectors $\mathbf{v}_i$ of H [52, 23]. Namely, $\forall\, i$ we can write:

$$\tilde{\mathbf{v}}_{ij} = c_i \mathbf{v}_{ij} \quad j \in S \tag{3.9}$$

where, by v_{ij} we denote the eigenvector components, while c_i corresponds to a normalization constant. That means, that each eigenvector of the reduced matrix is up to a normalization constant, the projection of the corresponding eigenvectors of H onto the set S.

3.3.1 Latent Symmetry

We are now ready to present the concept of latent symmetry that was recently introduced by Smith and Webb [113]. It was defined in the following way: A graph G has a latent symmetry, if there exists a subset of vertices S, that are symmetric under some isospectral reduction $R_S(G)$ [113]. Latent symmetry, as the name implies, allows one to identify symmetries of a network that are difficult to unravel unless performing a reduction.

To serve our purpose of connecting this notion to the phenomenon of perfectly transferring a state in a quantum network, we will consider isospectral reductions on a subset of two vertices. We say that two vertices are latently symmetric if their isospectral reduction is a bisymmetric matrix. When the adjacency matrix of the graph is symmetric,

which is always the case for the class of Hamiltonian matrices we consider in this work, the isospectral reduction over two vertices takes the following form:

$$R_S(H,\lambda) = \begin{pmatrix} f_1(\lambda) & g(\lambda) \\ g(\lambda) & f_2(\lambda) \end{pmatrix} \tag{3.10}$$

where $f_1(\lambda)$, $f_2(\lambda)$ and $g(\lambda)$ are rational functions of the parameter λ. Thus, in order for the matrix of Eq. 3.10 to be bisymmetric, we need $f_1(\lambda) = f_2(\lambda), \forall\lambda \in \mathcal{L}$.

If we look back at Eq. 3.9, we immediately notice that when two vertices of a Hamiltonian H are latently symmetric then the absolute values of the corresponding eigenvector components for each eigenvector of H should be equal to each other. Therefore, latent symmetry between two vertices implies cospectrality. This fact has been very recently demonstrated in [73].

3.3.2 4-site open chain revisited

Let us sum up the concepts introduced so far. A necessary condition between two vertices that support PST is that the corresponding eigenvector components for every eigenvector, should be equal to each other up to a sign. When this is the case, the two vertices are called cospectral. The notion of cospectrality has a geometrical interpretation in terms of walks on the quantum network. In fact, it implies that a not so apparent symmetry exists between the two vertices. A way to deduce whether this symmetry is present or not, is to perform the transformation of isospectral reduction. We will now demonstrate how to employ latent symmetry in order to identify the symmetry that has to be imposed on the J's profile in order to achieve PST between two vertices. To this purpose, we will consider the simple example of a 4-site open chain that was examined in the previous chapter.

The Hamiltonian matrix of a 4-site open chain is as follows:

$$H_4 = \begin{pmatrix} 0 & J_1 & 0 & 0 \\ J_1 & 0 & J_2 & 0 \\ 0 & J_2 & 0 & J_3 \\ 0 & 0 & J_3 & 0 \end{pmatrix} \tag{3.11}$$

We will first examine the transfers $1 \to 4$ and $1 \to 3$. In Eq. 3.12 we have calculated the isospectral reductions over the corresponding pairs of vertices.

$$R_{\{1,4\}}(H_4) = \begin{pmatrix} \frac{J_1^2\lambda}{\lambda^2-J_2^2} & \frac{J_1J_2J_3}{\lambda^2-J_2^2} \\ \frac{J_1J_2J_3}{\lambda^2-J_2^2} & \frac{J_3^2\lambda}{\lambda^2-J_2^2} \end{pmatrix} \quad R_{\{1,3\}}(H_4) = \begin{pmatrix} \frac{J_1^2}{\lambda} & \frac{J_1J_2}{\lambda} \\ \frac{J_1J_2}{\lambda} & \frac{J_2^2+J_3^2}{\lambda} \end{pmatrix} \tag{3.12}$$

When we demand that the resulting matrices should be bisymmetric for the case $1 \to 4$, we get that $J_1 = J_3$. This comes is accordance with the mirror symmetric profile that should be imposed on the chain in order to support PST between the first and the last vertices. On the other hand, for the transfer $1 \to 3$ we get a pythagorian triplet

$J_1^2 = J_2^2 + J_3^2$. Thus, an underlying hidden symmetry is revealed explaining the non mirror-symmetric profile of the couplings that we obtained in the previous chapter.

$$R_{\{1,2\}}(H_4) = \begin{pmatrix} 0 & J_1 \\ J_1 & \frac{J_2^2\lambda}{\lambda^2 - J_3^2} \end{pmatrix} \tag{3.13}$$

As for the case of the transfer $1 \to 2$, by inspecting the reduction of Eq. 3.13, we can immediately see that the only solution is $J_2 = 0$. Therefore, we can deduce that this transfer is non-reachable, since the only way to make the two vertices latently symmetric is to disconnect the chain.

3.4 What about network degeneracies?

We will now re-derive the necessary and sufficient conditions for PST, however on the contrary to the previous chapter, we will not assume that the system's eigenvalues are simple. Instead, we will consider the more general case where a degenerate eigenvalue $\mathcal{E}$ of multiplicity j exists. The following approach holds for an arbitrary number of degenerate multiplets.

We start by demanding PST between vertices n and m, of an N vertex graph, at the retrieval time t^*:

$$e^{-iHt^*} |n\rangle = e^{i\xi} |m\rangle \tag{3.14}$$

After inserting the resolution of unity, we split each sum to a degenerate and a non-degenerate subspace:

$$e^{i\mathcal{E}t^*} \sum_j \langle v_j'|n\rangle |v_j'\rangle + e^{iE_kt^*} \sum_k \langle v_k|n\rangle |v_k\rangle = e^{i\xi} \sum_j \langle v_j'|m\rangle |v_j'\rangle + e^{i\xi} \sum_k \langle v_k|m\rangle |v_k\rangle \tag{3.15}$$

where $|v_j'\rangle$ and $|v_k\rangle$ are the eigenvectors corresponding to the degenerate and the non-degenerate subspace respectively. Moreover, k is the number of simple eigenvalues and of course $N = j+k$. Invoking the linearly independence, we can treat the two subspaces independently. Thus, we obtain the two following equations:

$$e^{i\mathcal{E}t^*} \langle v_j'|n\rangle = e^{i\xi} \langle v_j'|m\rangle \tag{3.16}$$

$$e^{iE_kt^*} \langle v_k'|n\rangle = e^{i\xi} \langle v_k'|m\rangle \tag{3.17}$$

For the non-degenerate subspace we get:

$$\sin(E_kt^* - \xi) = 0 \quad \text{and} \quad \cos(E_kt^* - \xi) \langle v_k|n\rangle = \langle v_k|m\rangle \tag{3.18}$$

and combining the above results we have:

$$\langle v_k|n\rangle = d_k \langle v_k|m\rangle \tag{3.19}$$

where for a given k, d_k can be either $+1$ or -1. For the degenerate subspace we get:

$$\sin(\mathcal{E}t^* - \xi) = 0 \quad \text{and} \quad \cos(\mathcal{E}t^* - \xi) \langle v_j'|n\rangle = \langle v_j'|m\rangle \tag{3.20}$$

and we end up with:

$$\langle v'_j|n\rangle = d\,\langle v'_j|m\rangle \tag{3.21}$$

where in contrast to the previous case, for all j, d can be either $+1$ or -1. In other words, the relative sign of the eigenvector components corresponding to the vertices n and m, should be the same for every eigenvector belonging to the same degenerate subspace. Vertices satisfying the aforementioned condition are called strongly cospectral [63] due to the fact that the condition 3.21 is more restrictive than cospectrality. Moreover, in [73] it was proven that two vertices are strongly cospectral if and only if their isospectral reduction is a bisymmetric matrix and its eigenvalues are simple.

We will now present an indicative example employing strong cospectrality to achieve PST. We will consider a graph of five vertices and ten edges. The graph is depicted in Fig. 3.4 along with the corresponding Hamiltonian matrix. We will examine the case where the weights are determined by three parameters (a, b, c), all of which are different from each other. In this particular setting the Hamiltonian has a double degenerate eigenvalue $E_1 = E_2 = -a$. If we perform the isospectral reduction over all pairs of vertices, we can deduce that the following pairs are cospectral:

$$\{\mathrm{v}_1, \mathrm{v}_2\}, \quad \{\mathrm{v}_1, \mathrm{v}_3\}, \quad \{\mathrm{v}_2, \mathrm{v}_3\}, \quad \{\mathrm{v}_4, \mathrm{v}_5\} \tag{3.22}$$

However, when we run our optimization algorithm in order to find out whether a set of parameters $\{a, b, c, t^*\}$ exists such that PST is supported, we conclude that such a set exist only for the vertices $\{\mathrm{v}_4, \mathrm{v}_5\}$. This is because the vertices v_4 and v_5 are the only pair of strongly cospectral vertices, which becomes apparent when we calculate the spectrum of the reduced matrix:

$$R_{\{4,5\}} = \begin{pmatrix} \frac{3c^2}{\lambda-2a} & \frac{3c^2}{\lambda-2a} + b \\ \frac{3c^2}{\lambda-2a} + b & \frac{3c^2}{\lambda-2a} \end{pmatrix} \tag{3.23}$$

In every other case, the spectrum of the reduced matrices always contains the degenerate pair of eigenvalues. On the contrary, $\sigma(R_{\{4,5\}})$ does not contain any of the degenerate eigenvalues, both of them belong to the set $\sigma(H_{\bar{S}\bar{S}})$. In general, in order for two vertices to be strongly conspectral for a d-fold degenerate eigenvalue, at least $d-1$ eigenvalues should be contained in $\sigma(H_{\bar{S}\bar{S}})$. Let as return to the picture that was introduced in the previous chapter, where the exponential terms e^{iE_it} appearing in the sum:

$$F = \left| \sum_{i=1}^{5} v_{i4} v_{i5} e^{iE_i t} \right|^2, \tag{3.24}$$

are represented on the unit circle. In Fig. 3.4 we may notice that all vectors are aligned (red ones), besides two (black ones) which correspond to the degenerate eigenvalue. This may seem disturbing at first sight, since we have explicitly argued that in order for PST to occur all vectors should be aligned, so that the exponents can produce an overall sign that maximizes the fidelity. However, before rushing into conclusions, let us turn our attention on the eigenvector matrix of the Hamiltonian (computed for the set

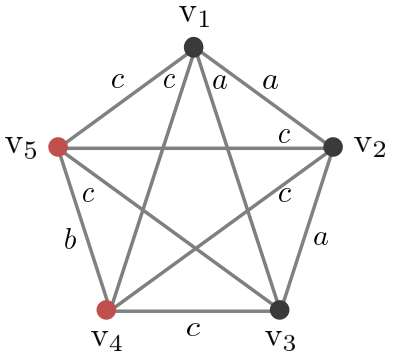

$$H = \begin{pmatrix} 0 & a & a & c & c \\ a & 0 & a & c & c \\ a & a & 0 & c & c \\ c & c & c & 0 & b \\ c & c & c & b & 0 \end{pmatrix}$$

Figure 3.4: A 5-vertex graph is given together with its Hamiltonian matrix. For this given parametrization of the edges, PST is only supported between vertices v_4 and v_5 which are strongly cospectral.

of parameters that result in PST between the fourth and the fifth vertices):

$$\begin{pmatrix} -0.8082 & 0.1158 & 0. & 0.3515 & -0.4579 \\ 0.5044 & 0.642 & 0. & 0.3515 & -0.4579 \\ 0.3038 & -0.7578 & 0. & 0.3515 & -0.4579 \\ 0. & 0. & -0.7071 & -0.5608 & -0.4305 \\ 0. & 0. & 0.7071 & -0.5608 & -0.4305 \end{pmatrix} \tag{3.25}$$

where the first two columns are the two eigenvectors corresponding to the degenerate eigenvalues. One can immediately notice that the eigenvector components corresponding to the fourth and the fifth site (v_{14}, v_{15} and v_{24}, v_{25}) are equal to zero. Thus, these two terms contribute to the maximization of the sum of Eq. 3.24, through their absence and due to this reason the corresponding vectors in Fig. 3.4 do not have to be aligned with the rest. In the general case, strong cospectrality ensures that the exponetial factor of the degenerate subspace aligns the corresponding vectors, at $t = t^*$, with the rest.

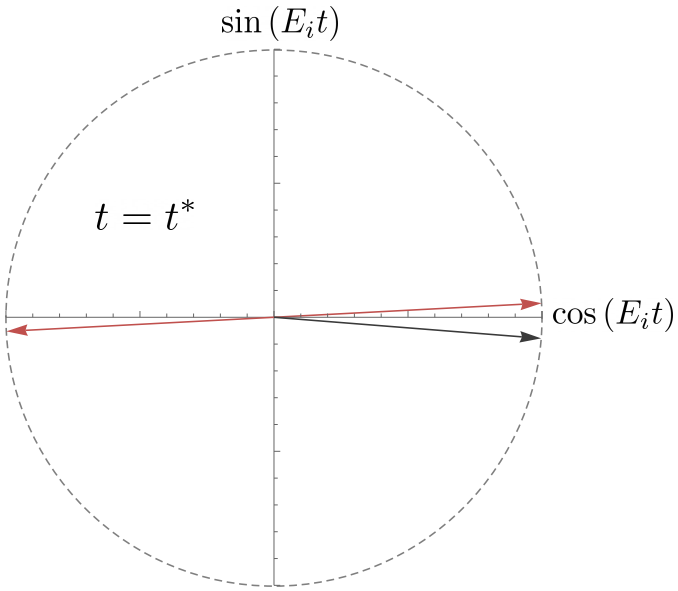

Figure 3.5: The exponential terms e^{iE_it} for the example we considered in Fig. 3.4 are represented as vectors on the unit circle for $t = t^*$, where PST occurs.

3.5 Applicability

In this chapter we have unraveled the connections between the PST in engineered chains and some recently developed concepts coming from graph theory. By doing so, we have traced the origin of both symmetric and asymmetric profiles that we encountered in the previous chapter when examining open and closed geometries. The underlying symmetry a network should posses, in order to support PST between a pair of vertices, is the latent symmetry. The isospectral reduction procedure provides a straightforward methodology, that allows us to deduce whether the aforementioned symmetry is present in a quantum network. Moreover, we are able to obtain the symmetries of the couplings' profile. This information is crucial for both the optimization and the inverse eigenvalue algorithms [69], which are the main numerical tools that are employed for designing networks that support PST. Lastly, in a given network where the geometry of the network does not allow for PST to occur, schemes can be devised to obtain the set of suitable modifications that have to be applied in order to make it so. Steps towards this direction have been made in [63, 106, 88].

Chapter 4

Fractional State Transfer

4.1 Preliminaries

A way to generate entanglement in the one-excitation subspace of a quantum spin channel through the engineered J's protocol is by employing the phenomenon of fractional revival. As we have already seen in Chapter 2, when a one-site excitation at some point during the dynamical evolution relocalizes on the initial site, we say that a revival has occurred. The fractional revival on the other hand, occurs when the wavefunction, for a time t^* in between two revivals, is localized in a particular number of sites (target sites). This phenomenon exhibits a periodic behavior with period equal to the period of one full revival. In fact from a point of view, PST can be thought of, as a special case of fractional revival.

Coming back to entanglement, it is worth noting that since the early days of the engineered protocol, it was highlighted [38] that entanglement transfer can be realized in the chain. In the most simple case, this is due to the fact that the mirror symmetric profile simultaneously supports PST between mirror symmetric sites. We can imagine that a Bell state of the form $1/\sqrt{2}(|01\rangle + |10\rangle)$ is imposed on the first two qubits of an N-site chain. Therefore, in the one excitation subspace (i.e. $|k\rangle = |0_1 0_2 ... 1_k ... 0_{N-1}\rangle$) our initial state has the form

$$|\psi(t=0)\rangle = \frac{1}{\sqrt{2}}(|1\rangle + |2\rangle) \tag{4.1}$$

At $t = t^*$, corresponding to the retrieval time where PST occurs between vertices $1 \to N$ and $2 \to N-1$ we will get the state

$$|\psi(t=t^*)\rangle = \frac{1}{\sqrt{2}}(|N\rangle + |N-1\rangle) \tag{4.2}$$

In this way, the Bell state is transferred on the other end of the chain. An important thing that we have to keep in mind and also applies for the fractional revivals we will consider in this chapter, is the fact that since we restrict ourselves to the one-excitation subspace,

we do not consider entangled states containing two-excitation terms like $1/\sqrt{2}(|00\rangle + |11\rangle)$.

In the same spirit with the aforementioned scheme, one can consider the following scenario. We start with an excitation localized on the first site of the chain $|1\rangle$. If the chain supports a fractional revival, where the wavefunction is equally distributed among the first and the last site, at t^* we obtain the state $1/\sqrt{2}(|1\rangle + |N\rangle)$. Tracing out the other spins of the chain, this is equivalent to the generation of the entangled state $1/\sqrt{2}(|10\rangle + |01\rangle)$. In fact a few years back, Kay [71] generalized this approach by numerically demonstrating that in principle, an arbitrary one excitation quantum state can be generated by suitably engineering the quantum channel.

In this chapter we will present our contribution towards the direction of entanglement generation in an engineered quantum channel. We will do so by extending the approach we followed in Chapter 2. In this case, we will examine the splitting of the wavefunction during the transfer between an arbitrary initial and two arbitrary target sites of the spin chain. When this transfer process occurs with fidelity $F = 1$, we say that Fractional State Transfer (FST) has occurred. We will consider the fractional revivals as a special case of FST, corresponding to the case where one of the target sites is the same as the initial one. Our aim is to identify the reachable and non-reachable transfers and deduce which states can be prepared by employing this scheme.

4.2 Reachability criteria for FST

We yet again restrict ourselves to the one-excitation subspace of the XX Hamiltonian (see Eq. 2.2) and we are considering the transfer between an initial site $|n\rangle$ and two target sites $|m\rangle$ and $|k\rangle$. The target state has the following form:

$$|\psi(t = t^*)\rangle = \cos\chi\,|m\rangle + \sin\chi e^{i\theta}\,|k\rangle \tag{4.3}$$

where $\chi \in (0, \pi/2)$ and $\theta \in [0, 2\pi)$ In order to achieve fractional perfect state transfer, the following equation should hold:

$$e^{-iHt^*}\,|n\rangle = e^{i\xi}(\cos\chi\,|m\rangle + e^{i\theta}\sin\chi\,|k\rangle) \tag{4.4}$$

inserting the resolution of identity we get:

$$\sum_{i=1}^{N} e^{i(E_i t^* - \xi)}\,\langle v_i|n\rangle\,|v_i\rangle = \sum_{i=1}^{N}(\cos\chi\,\langle v_i|m\rangle + e^{i\theta}\sin\chi\,\langle v_i|k\rangle)\,|v_i\rangle \tag{4.5}$$

and invoking linear independence:

$$e^{i(E_i t^* - \xi)}\,\langle v_i|n\rangle = \cos\chi\,\langle v_i|m\rangle + e^{i\theta}\sin\chi\,\langle v_i|k\rangle\,, \quad \forall i. \tag{4.6}$$

Thus, when separating real and imaginary parts we end up with the following relations:

$$\cos(E_i t^* - \xi)\,\langle v_i|n\rangle = \cos\chi\,\langle v_i|m\rangle + \cos\theta\sin\chi\,\langle v_i|k\rangle \tag{4.7a}$$

$$\sin(E_i t^* - \xi)\,\langle v_i|n\rangle = \sin\theta\sin\chi\,\langle v_i|k\rangle \tag{4.7b}$$

From here on, we can distinguish two cases, one where $\theta = \nu\pi$ for which we obtain:

$$\sin(E_i t^* - \xi) = 0 \tag{4.8a}$$

$$\langle v_i|n\rangle = \pm(\cos\chi\,\langle v_i|m\rangle + \sin\chi\,\langle v_i|k\rangle) \tag{4.8b}$$

and another where $\theta \neq \nu\pi$, for which we get:

$$\sum_{i=1}^{N} \frac{\sin^2(E_i t^* - \xi)}{\sin^2\theta \sin^2\chi} = 1 \tag{4.9a}$$

$$\sum_{i=1}^{N} \frac{\sin^2(\theta - E_i t^* + \xi)}{\sin^2\theta \cos^2\chi} = 1 \tag{4.9b}$$

What we can immediately notice, is that for $\theta = \nu\pi$ we once more obtain the rationality criterium (see Eq. 4.8(a)), that we have encountered in the PST case of Chapter 2.

4.3 Numerical results

In a manner similar to Chapter 2, an optimization algorithm was employed to examine the reachable and non-reachable transfers in an open chain geometry. The optimization parameters are the couplings J_i, time t, the relative phase between the two targets θ and the angle χ, which is related to the target sites' amplitudes. The cost function that the optimization algorithm tries to minimize is the infidelity, defined as $1 - F$, where F is the fidelity of FST given by:

$$F = \left|\langle\psi(t = t^*)|\, e^{-iHt}\, |n\rangle\right|^2 \tag{4.10}$$

We will start by sketching the pattern of reachable and non-reachable transfers based on our numerical results. Even and odd-sized chains will be treated separately.

Concerning the even-sized chains, fractional revivals are always reachable when $n = m$ and k is the mirror symmetric of m. In these cases $\theta = \frac{\pi}{2}$ and the J's profile are symmetric. The fractional revival between the first and the $N - 1$ site of the chain is also always reachable. All transfers where the target sites are 1 and N are reachable, irrespective of the initial site. Finally, in general, the transfers where both target sites are in the first half of the chain ($m, k \leq N/2$) are non-reachable.

For odd-sized chains, all transfers where the target sites are 1 and N are reachable, irrespective of the initial site. In addition, every transfer where $n = 1$, $m = i (i = 1, 2, ..., N - 1)$ and $k = N$, is reachable . Non-reachable are the transfers where we go from the central site to the two nearest mirror symmetric ones, an exception to this rule is $N = 3$ where FST is supported and the two couplings are equal to each other $J_1 = J_2$. Finally, similarly to the even-sized chains, the only fractional revivals that are reachable are the ones where the initial site n ($n = m$) and the target site k are mirror

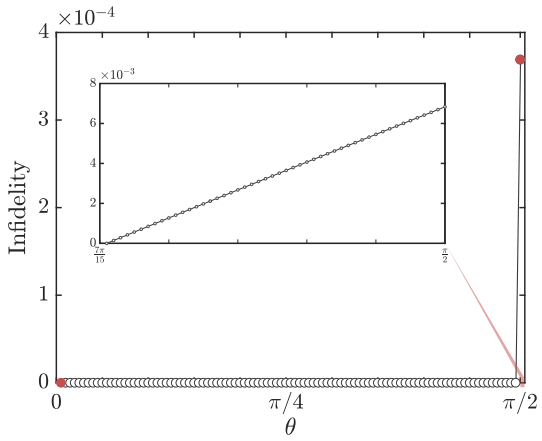

Figure 4.1: Infidelity as a function of the angle χ, corresponding to the fractional state transfer $1 \rightarrow 4 + 2$. The red points correspond to the values $\chi = 0$ (PST between 1 and 4) and $\chi = \pi/2$ (non-reachable PST between 1 and 2). The inset shows the gradual increase of infidelity in the region close to $\pi/2$.

symmetric. Note, that in this case, in contrast with the even-sized chains, the relative phase is $\theta = \nu\pi$.

We will highlight some important aspects of the aforementioned numerical results. One thing that we examined is how the solutions we obtain are affected by the amplitudes of the target sites. More specifically, we wanted to know if there are values of the parameter χ for which the infidelity of the process is increased. To this purpose for the reachable transfers we have taken different values of $\chi \in [0, \pi/2]$ and for each value we obtained through the optimization algorithm the optimal set of parameters that minimizes the infidelity. In Fig. 4.1, we give an indicative example by considering the fractional state transfer between the initial site $|1\rangle$ and the target sites $|2\rangle$ and $|4\rangle$. For $\chi = 0$ the infidelity of the process is zero (i.e. of the order of 10^{-16}) since this corresponds to PST between the first and the fourth site, which we know is reachable. On the contrary for $\chi = \pi/2$, which corresponds to the non-reachable transfer between sites 1 and 2, the infidelity is increased and becomes of the order of 10^{-4}. For the rest of the values corresponding to different distributions of the wavefunction among the target sites the infidelity is zero. This fact indicates that the process is insensitive to the values of the amplitudes that we may impose on the target state. Let us make one small remark here concerning Fig. 4.1. The fact that in the infidelity suddenly jumps when approaching the value $\chi = \pi/2$, is due to the size of the step we have chosen for scanning the interval. If we decrease the size of the step and examine the behavior of infidelity for χ-values arbitrary close to $\pi/2$ we will see that the transition is smooth and no sudden jump takes place (see the inset in Fig. 4.1).

Of particular interest is the profile where all J's, besides the ones on the center of the chain, are mirror symmetric. Solutions that follow this profile have been first obtained in [44] and later on in [10] through an inverse eigenvalue schemes, while in [58] an analytical treatment was developed. In every case, their relation to the mirror profile

of the standard PST has been highlighted. We have strong numerical indications that this is a distinct feature of fractional revivals, since no such profile for the couplings has been encountered in any other fractional state transfer process.

Lastly our attention was drawn by the fact that in order to get zero infidelity the phase factor θ is restricted in acquiring either the value $\nu\pi$ or $(2\nu+1)\frac{\pi}{2}$, where $\nu \in \mathbb{Z}$. To validate this numerically, for fixed amplitudes (i.e. χ) we have examined infidelity's behavior, taking the phase factor $\theta \in [0, 2\pi]$. In Fig. 4.2 we consider two such examples. On the right plot it is apparent that in order to get zero infidelity, the phase factor θ has to be equal to $\nu\pi$, while on the left plot $\theta = (2\nu+1)\frac{\pi}{2}$. Examining the pattern of reachable transfers we have observed that if the two target sites are both odd or even-labeled the relative phase $\theta = \nu\pi$ (e.g. Fig. 4.2(a)). On the other hand, when one target site is even and the other odd we get $\theta = (2\nu+1)\frac{\pi}{2}$ (e.g. 4.2(b)). In the following section we will analytically demonstrate that this is the case for a particular class of networks which are called bipartite.

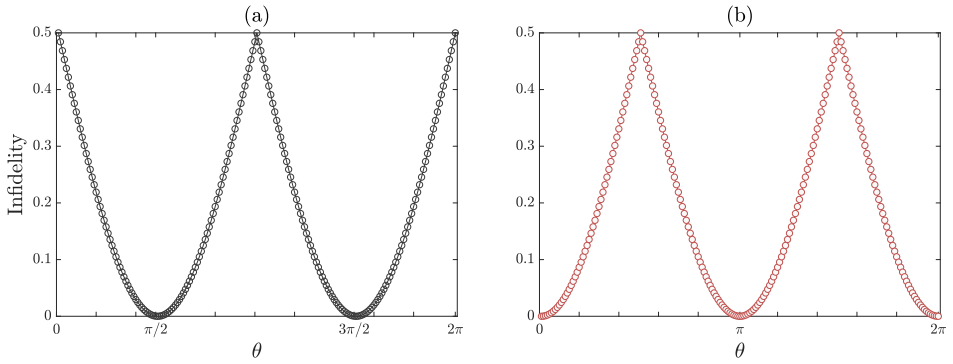

Figure 4.2: Infidelity as a function of the angle θ, corresponding to the fractional state transfer (a) $1 \to 1+4$ and (b) $1 \to 2+4$.

4.4 Restrictions on the relative phase

In this section we will analytically demonstrate why the relative phase between the two target sites that were considered, is restricted in acquiring the values $\theta = \nu\pi$ or $(2\nu+1)\frac{\pi}{2}$. To this purpose, we will first introduce the notion of a bipartite graph [62]. A graph is bipartite if all its vertices can be partitioned in two sets S_1 and S_2, in such a way that every edge has one end belonging to S_1 and the other to S_2. A way to identify the bipartite character of a graph is through proper coloring. Proper coloring is the procedure where colors are assigned on each vertex, such that no adjacent vertices have the same color. Of course for a N-vertex graph this can be trivially realized by employing N different colors. What is important is the least number of colors that are needed for proper coloring a graph. This number is called the chromatic number of a graph. If the chromatic number of a graph is 2 then the graph is bipartite. In Fig. 4.3 we provide some examples of bipartite and non-bipartite graphs.

For a bipartite Hamiltonian matrix, assuming that its vertices are colored with black and red, we can define [100] the operator:

$$S = \sum_{n\in\text{black}} |n\rangle\langle n| - \sum_{n\in\text{red}} |n\rangle\langle n| \tag{4.11}$$

which anticommutes with the Hamiltonian. For an open chain, we assign the black color to even-numbered vertices and the red to odd-numbered vertices. If k is an even vertex $S|k\rangle = |k\rangle$, while if k is an odd vertex $S|k\rangle = -|k\rangle$. Moreover, for every eigenvector $|v_i\rangle$ with eigenvalues E_i, $S|v_i\rangle$ will be the eigenvector corresponding to the eigenvalue $-E_i$. Based on the latter, we can write:

$$e^{iHt^*}|n\rangle = \sum_{E_i>0} \langle v_i|n\rangle \left(e^{-iE_it^*}|v_i\rangle + e^{iE_it^*}S|v_i\rangle\right) \tag{4.12}$$

where $|v_i\rangle$ are the eigenvectors corresponding to the positive eigenvalues. If we multiply Eq. 4.12 from the left by a site basis vector $\langle k|$ depending on whether k is even or odd, the sign of the second term inside the sum will be plus or minus respectively. Thus, for $k \in$ even, $\langle k|\, e^{iHt^*}|n\rangle$ will become a sum of cosines Eq. 4.13 (a). On the contrary for

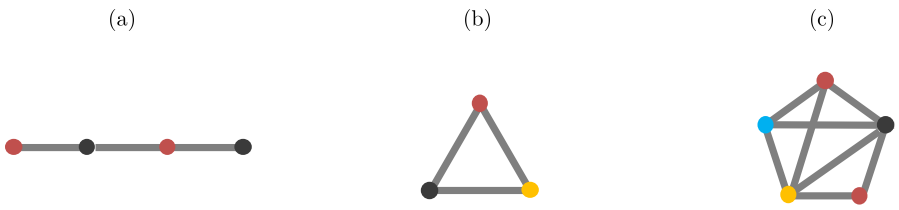

Figure 4.3: (a) A bipartite graph with chromatic number 2. (b) A graph with chromatic number 3 (c) A graph with chromatic number 4.

$k \in$ odd, we will get a purely imaginary sum of sines Eq. 4.13 (b).

$$\langle k_{\text{even}}| e^{iHt^*} |n\rangle = 2 \sum_{E_i>0} \langle v_i|n\rangle \langle k_{\text{even}}|v_i\rangle \cos(E_i t^*) \tag{4.13a}$$

$$\langle k_{\text{odd}}| e^{iHt^*} |n\rangle = -2i \sum_{E_i>0} 2 \langle v_i|n\rangle \langle k_{\text{odd}}|v_i\rangle \sin(E_i t^*) \tag{4.13b}$$

The same equation will of course hold if instead of $k_{\text{even}}, k_{\text{odd}}$ we had $m_{\text{even}}, m_{\text{odd}}$. On the other hand, when we multiply Eq. 4.4 from the left with $\langle k|$ and $\langle m|$ we get:

$$\langle k| e^{iHt^*} |n\rangle = \cos(\theta+\xi)\sin\chi + isin(\theta+\xi)\sin\chi \tag{4.14a}$$

$$\langle m| e^{iHt^*} |n\rangle = \cos\xi\cos\chi + i\sin\xi\cos\chi \tag{4.14b}$$

If we now equate the real and imaginary parts of Eq. 4.13 and Eq. 4.14 for both $k_{\text{even}}, k_{\text{odd}}$ and $m_{\text{even}}, m_{\text{odd}}$ we can derive the following relations:

$$k_{\text{even}}, m_{\text{even}}: \quad \sin(\theta+\xi)=0 \quad \text{and} \quad \sin\xi = 0 \tag{4.15a}$$

$$k_{\text{odd}}, m_{\text{odd}}: \quad \cos(\theta+\xi)=0 \quad \text{and} \quad \cos\xi = 0 \tag{4.15b}$$

$$k_{\text{odd}}, m_{\text{even}}: \quad \cos(\theta+\xi)=0 \quad \text{and} \quad \sin\xi = 0 \tag{4.15c}$$

$$k_{\text{even}}, m_{\text{odd}}: \quad \sin(\theta+\xi)=0 \quad \text{and} \quad \cos\xi = 0 \tag{4.15d}$$

From which it directly follows that for a bipartite Hamiltonian, when the two target sites belong to the same partition of vertices, their relative phase is restricted to take the values $\theta = \nu\pi$, while when they belong to different partitions $\theta = (2\nu+1)\pi/2$, where $\nu \in \mathbb{Z}$. This proof can be seen as an extention of the approach developed by Kay in [70], where the bipartite nature of the chain was related to PST.

4.5 Reachability criteria for bipartite networks

Having addressed the restrictions that are imposed on the relative phase, let us revisit the analytic relations that were derived in Section 4.2. For simplicity, let us only consider the case where the wavefunction equally splits between the two target sites (i.e. $\chi = \pi/4$). We hereby present the reachability criteria for FST in terms of the eigenvalues and the eigenvector components of the Hamiltonian.

For $\theta = \nu\pi$ from Eq. 4.8 we get:

$$\sin(E_i t^* - \xi) = 0 \tag{4.16a}$$

$$\langle v_i|n\rangle = \pm\frac{1}{\sqrt{2}}(\langle v_i|m\rangle + \langle v_i|k\rangle) \tag{4.16b}$$

due to the bipartite nature of the spin chain the rationality criterium (Eq. 4.16(a)) implies that the retrieval time t^* can be chosen appropriately, such that the eigenvalues acquire integer values, while Eq. 4.16(a) describes the relation between the eigenvector components of the sites that participate in the fractional transfer process.

On the other hand, for $\theta = (2\nu + 1)\pi/2$ we get the following equations:

$$\sum_{i=1}^{N} \sin^2(E_i t^* - \xi) = \frac{1}{2} \tag{4.17a}$$

$$\langle v_i|m\rangle = \sqrt{2}\cos\left(E_i t^* - \xi\right)\langle v_i|n\rangle \tag{4.17b}$$

$$\langle v_i|k\rangle = \sqrt{2}\sin\left(E_i t^* - \xi\right)\langle v_i|n\rangle \tag{4.17c}$$

In contrast to the PST case, due to the complexity of the above equations, we have not yet identified a geometrical symmetry of the network that can be related to Eq. 4.16 (b) and Eq. 4.17 (b) and (c).

Chapter 5

A time-driven quantum channel

5.1 Preliminaries

In the previous chapters we have turned our focus on the engineered J's protocol. We have seen that the major advantages of this protocol are the high speed of information transfer and the fact that no dynamical control is needed during the transfer process. However, besides the speed of the transfer, there is another factor that determines the efficiency of the transfer process and that is the protocols resilience to different sources of decoherence. In addition to that, we have seen that PST occurs in between two revivals of the initial state where the fidelity of the transfer forms a peak. Thus, a crucial aspect in order to achieve a high fidelity transfer is to be able to read out the target state at a particular time window related to the width of the peak. The latter feature is present in various QST protocols and poses a challenging task for the experimentalists.

An alternative approach aiming to properly address one or both of the aforementioned issues, are time-dependened quantum protocols. In this approach, the parameters of the quantum channel are time-driven during the transfer process. As we already mentioned in the introduction, the most intuitive way of realizing a time-dependent protocol is to perform a series of swap operations in order to gradually move the excitation site by site until the target state is reached. Although, this protocol performs well in terms of speed, when disorder is introduced on the system's parameters, the fidelity of the transfer is highly degraded. This effect was highlighted in [103], where a comparison, in terms of the effect of disorder, was made between the engineered "static" protocol and one adiabatic time-dependent transfer protocol. It was deduced that although the static quantum channel by far outperforms the adiabatic one in terms of speed, it is more susceptible to static off-diagonal noise in J's. In most cases, increasing the speed comes along with a decrease in terms of robustness. Therefore, finding the balance between these two aspects is a task of crucial importance.

A very active research direction that was initiated the past few years, employs systems that possess topological characteristics to develop efficient QST protocols. These

systems, due to their topological protection, are extremely resilient to specific sources of decoherence. In this chapter we will examine a QST protocol employing a Su-Schrieffer-Heeger (SSH) chain, revealing crucial aspects of the driving function that when handled appropriately, lead to fast and robust transfer process. To demonstrate this, we will make a comparison between our proposal and another time-dependent protocol, in which the underlying undriven quantum channel is topologically trivial.

5.1.1 SSH model

We will start by briefly introducing the SSH model. We will hereby present only the properties that will be necessary to our discussion. For a more detailed review of the model we refer the reader to [4]. The SSH chain is the simplest topologically non-trivial system in 1-D that can be obtained by suitably modifying the Hamiltonian of the one excitation subspace that was introduced in Chapter 2:

$$\mathcal{H} = \sum_{i=1}^{N-1} J_i(|i\rangle \langle i+1| + h.c.) + \sum_{i=1}^{N} B_i |i\rangle \langle i| \tag{5.1}$$

To do so, the chain has to be dimerized. Meaning, we have to make $J_i = J_{odd}$ for $i \in odd$ and $J_i = J_{even}$ for $i \in even$. In addition, the magnetic field needs to be constant. We will once again assume that $B_i = 0 \; \forall i$, unless explicitly stated otherwise. We will distinguish two cases, one where the SSH chain consists of an even number of sites $N \in even$ and another where $N \in odd$.

For even-sized chains the topological phase arises when $J_{odd} < J_{even}$ and two modes appear at the center of the energy gap (see Fig. 5.1). On the contrary, in the trivial phase where $J_{odd} > J_{even}$ no modes appear inside the gap. The energies corresponding to the two eigenmodes lie close (above and below) to $E = 0$ and are separated from the rest of the modes by a finite energy gap of the order of J_{even}. This gap is a characteristic feature of topological protection. If we construct a linear combination of the two eigenvectors corresponding to the two modes, we obtain a state that is localized on the left $|L\rangle$ or on the right side $|R\rangle$ of the chain depending on the relative sign between the two eigenvectors (see Fig. 5.1).

If we initially prepare the system to be the state that is localized on the left side of the chain and we let it evolve freely, due to the finite size of the chain, the wavefunction of $|L\rangle$ has an overlap with $|R\rangle$. Thus, as the system evolves in time, there will be an Rabi-like oscillation between the states $|L\rangle$ and $|R\rangle$. This scheme has been employed to create an efficient time-independent QST protocol for transferring single site excitations along the chain [79, 54]. It closely resembles the weak-coupling (or strong- magentic field) protocols that have been proposed to create Rabi-like oscillation schemes for transferring excitations [122, 111, 84], but its additional topological protection makes it more robust to specific types of disorder. The drawback of this approach is that the energy spacing between the two modes is decreased (exponentially) as the length of the chain increases. Thus, leading to large transfer times as the systems' size scales up.

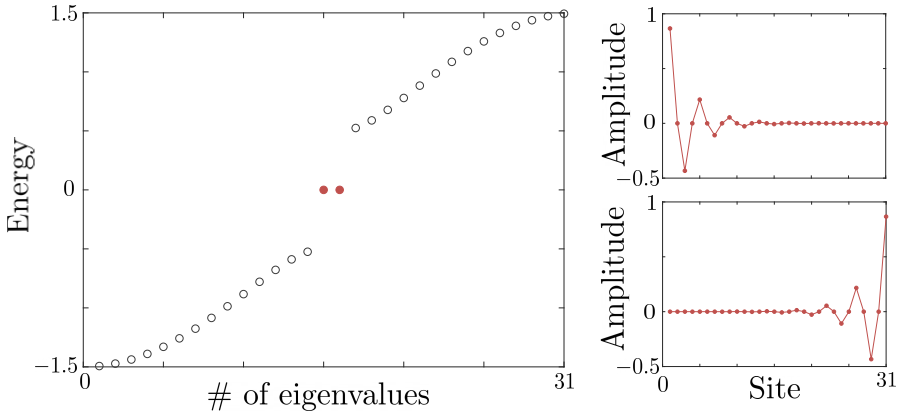

Figure 5.1: On the left we depict the spectrum of an even-sized SSH chain in its topological phase, consisting of $N = 30$ and where $J_{odd} < J_{even}$ ($J_{odd} = 0.5, J_{even} = 1$). On the right we have plotted the linear combinations of the two modes that are sitting in the middle of the energy gap ($|L\rangle$ on the top right panel and $|R\rangle$ on the bottom).

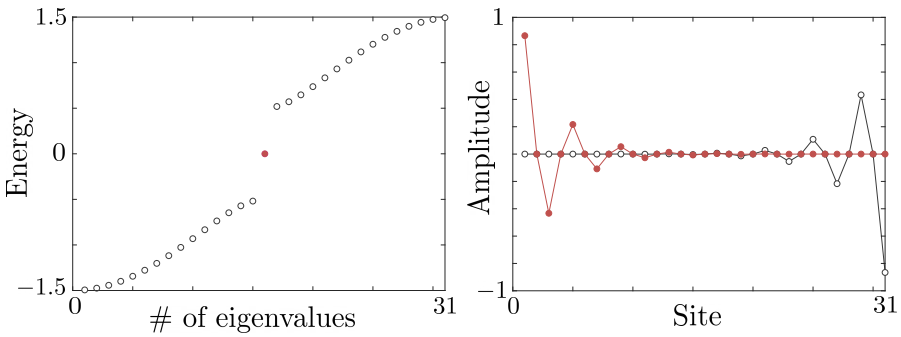

Figure 5.2: On the left we depict the spectrum of an odd-sized SSH chain, consisting of $N = 31$ and $J_{odd} = 0.5, J_{even} = 1.0$. On the right we have plotted the eigenvector corresponding to the zero mode. The red mode corresponds to $J_{odd} < J_{even}$, while the black to the exact opposite case, where $J_{odd} > J_{even}$.

On the contrary, for odd-sized chains, there is always one zero mode (see Fig. 5.2) that is localized on the end corresponding to the weaker coupling. Namely, when $J_{odd} < J_{even}$ ($J_{odd} > J_{even}$) the mode is localized near the first (last) site of the chain (see Fig. 5.2). In this case the energy of the mode is exactly zero. For odd-sized chains the eigenmode energies (besides the zero energy solution) are given by the following expression:

$$\epsilon_j = \pm\left|J_{odd} + J_{even}e^{iq_j}\right|, \tag{5.2}$$

where $q_j = 2j\pi/(N+1)$ and $j = 1, 2, ..., [N/2]$ (j counts the number of $\pm$ pairs and $[x]$ gives the greatest integer that is less than equal to x) [42]. Thus, for an odd-sized chain of length N the energy gap can be analytically determined and is given by:

$$g = 2\left|\epsilon_{[N/2]}\right| \tag{5.3}$$

The main protocol we will examine in this chapter is based on the odd-sized SSH chain.

5.2 QST protocols

The aim of the protocols we will consider, is to transfer a single excitation from the first $|1\rangle$ to the last $|N\rangle$ site of the chain, by properly controlling the couplings $J_i(t)$ during the dynamical evolution. The quantity that determines how faithfully the transfer has occurred is the fidelity, which for a time-dependent protocol can be defined as:

$$\mathcal{F} = |\langle N|N(t^*)\rangle|^2 \tag{5.4}$$

where by $|N(t^*)\rangle$ we denote amplitude of the N-th site, obtained by numerically solving the time-dependent Schrödinger equation and t^* corresponds to the transfer time. In all protocols we will present, the energy scale is determined by the maximum value that the couplings acquire during the dynamical evolution. Thus, without loss of generality we will set $J_{max} = 1$. Time will be given in units of $1/J_{max}$ and energy in units of J_{max}. We will now present two different cases for realizing an efficient time-driven quantum channel, one where the underlying undriven chain has topological characteristics and another where the chain is topologically trivial.

5.2.1 Topological chain

We restrict ourselves to odd-sized chains and we assume that we can separately control even and odd-indexed couplings. Initially the system is prepared so that $J_{odd} = 0$ and $J_{even} = 1$ and the excitation is localized on the first site of the chain which is disconnected from the rest (see Fig. 5.3 (a)). Therefore, the initial state is an eigenstate of the system ($|100...0\rangle$ with zero eigenenergy). At the transfer time t^* (see Fig. 5.3 (c)) we end up with the opposite situation (i.e. $J_{even} = 0$ and $J_{odd} = 1$). The system undergoes a transition and transforms from a topological chain supporting an edge mode on the first site, to a topological chain with an edge mode on the last site, resulting to

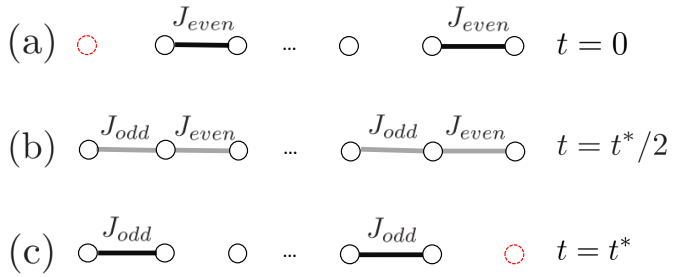

Figure 5.3: A schematic of different time instants during the dynamical evolution of the topological chain. (a) Initially, $J_{odd} = 0$, $J_{even} = J_{max}$, the zero-mode is localized on the first site and the energy gap takes its maximum value ($\sim J_{max}$). (b) For $t = t^*/2$ we have $J_{odd} = J_{even} = J < J_{max}$ and the energy gap acquires its minimum value ($\sim 4J/N$). Before and after $t^*/2$ we have $J_{odd} < J_{even} < J_{max}$ and $J_{even} < J_{odd} < J_{max}$ respectively. (c) Finally, $J_{odd} = J_{max}$, $J_{even} = 0$, the zero-mode is localized on the last site and the energy gap, once again takes its maximum value.

an excitation transfer from one side to the other. Note here, that in this protocol, there always exists a time where all the couplings acquire the same value $J_{even} = J_{odd}$. In our case we will consider this time to be $t = t^*/2$ (see Fig. 5.3 (b)). For the infinite system, $J_{even} = J_{odd}$ corresponds to the closing of the energy gap separating the zero-energy mode with the rest excited states. However, in finite systems a finite energy difference between any two modes is always present. Thus, the point in the parameter space where $J_{even} = J_{odd}$, corresponds to the minimization of the energy gap.

5.2.2 Topologically-trivial chain

To explore how the topological nature of the underlying static chain affects the transfer, we will proceed to a comparison with a protocol employing a topologically-trivial chain. We consider a protocol where the only couplings that are controlled are the ones connecting the edge sites with the rest of the chain (i.e. J_1 and J_{N-1}). This protocol has been chosen based on its performance in terms of speed and also by the fact that local manipulation of the system's parameters makes it experimentally more feasible. As was the case for the topological chain, the initial state is localized at the first site and corresponds to the system's zero-energy eigenstate (see Fig. 5.4 (a)). Here, $J_1 = 0$ while $J_i = J \; \forall i \neq 1$. During the dynamical evolution, due to the odd-size of the chain, the zero-energy eigenstate is always present. Therefore, gradually switching on J_1 while J_{N-1} is decreased, results at time t^*, to the transfer of the excitation at the other end of the chain (see Fig. 5.4 (c)). An important difference between this protocol and the one described in the previous section, is that in this case, there is no point in the parameter space where all the couplings acquire the same value.

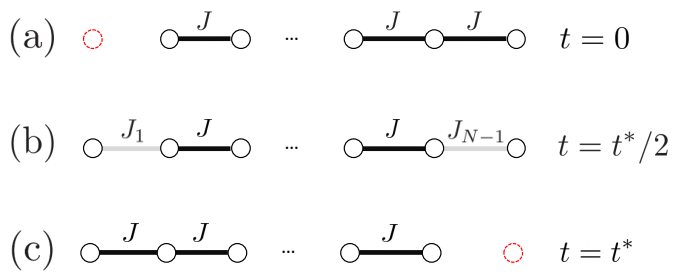

Figure 5.4: A schematic of different time instants during the dynamical evolution of the topologically-trivial chain. (a) Initially, $J_1 = 0$, $J_i = J_{max}$ where $i = 2, ..., N-1$, the zero-mode is localized on the first site and the energy gap takes its maximum value. (b) For $t = t^*/2$ we have $J_1 = J_{N-1} < J_{max}$ while $J_i = J_{max}$ for $i = 2, 3, ..., J_{N-2}$. Before and after $t^*/2$ we have $J_1 < J_{N-1} < J_{max}$ and $J_{N-1} < J_1 < J_{max}$ respectively. (c) Finally, $J_1 = 0$ and $J_i = J_{max}$ for $i = 2, ..., N-1$, while the zero-mode is localized at the last site of the chain.

5.3 Crucial characteristics of the driving function

Before presenting our numerical results, we will develop an intuitive and solid line of arguments that dictate which are the crucial considerations that have to be taken into account when driving the state transfer in an odd-sized SSH chain. In all protocols we will consider the system is prepared in the zero-energy eigenstate that is localized on the first site of the chain. As the system evolves, a zero-energy state is always present due to the odd size of the chain. Therefore, the adiabatic approximation ensures, that if the system is driven sufficiently slow during the transfer process, the system remains in the zero-energy eigenstate without exciting eigenstates. Our proposal is based on suitably adjusting the driving function in order to reach high fidelity values for small transfer times. Our approach does not rely on methods like the adiabatic passage or shortcuts to adiabaticity, where specifically engineered terms are introduced in the Hamiltonian that can induce counter-processes able to suppress the excitations. In other words, we confine ourselves to drive the parameters of nearest-neighbor coupling. To introduce counter-adiabatic terms one should include next-to-nearest neighbor interactions like in [45].

When driving the chain, we focus on two important quantities: The energy difference between the zero-mode and the rest of the states, and the derivative of the Hamiltonian matrix that is directly related to the slope of the driving function. These two quantities, after all, appear in the definition of the adiabatic invariant [86], which goes as follows: Assuming that $|v_i(t)\rangle$ is the instantaneous the zero-energy eigenstate, in order to be close to the adiabatic limit, the following sum has to be sufficiently small

$$\sum_{j \neq i} \frac{\langle v_j(t)| \dot{\hat{H}} |v_i(t)\rangle}{E_j(t) - E_i(t)} \ll 1, \tag{5.5}$$

where $E_m(t)$ the instantaneous eigenenergy of the j^{th} mode and $\dot{\hat{H}}$ the time-derivative of the Hamiltonian. Equation 7.4 holds when no degeneracies appear in the spectrum

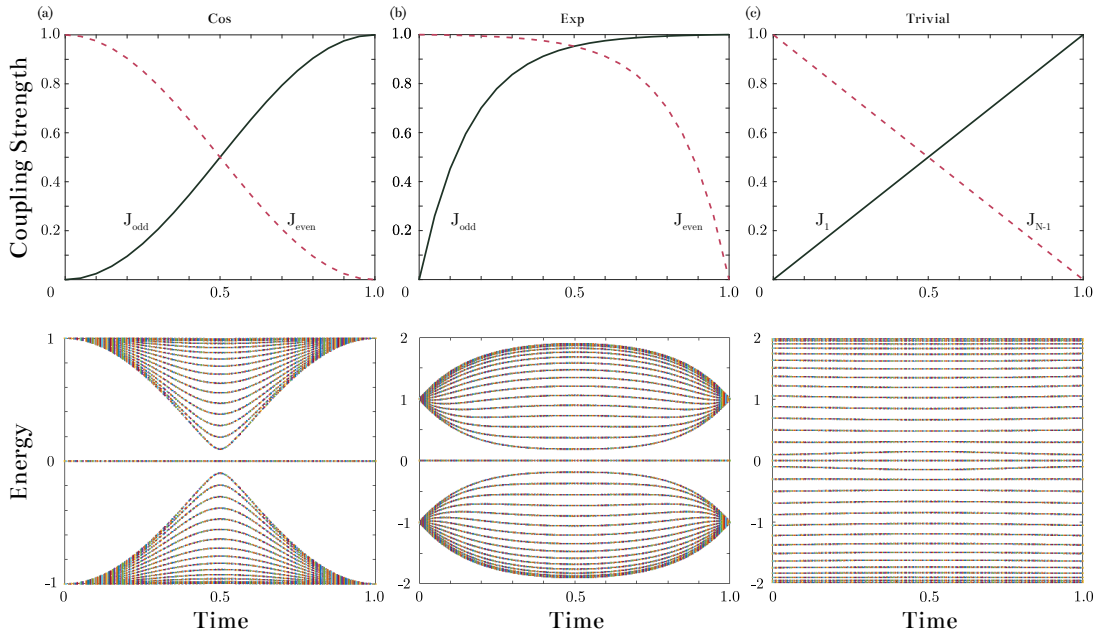

Figure 5.5: For each protocol (a) cosine (b) exponential and (c) trivial, on the top panel we plot the driving function as a function of time. While on the bottom panel, we depict the corresponding instantaneous energy spectrum as a function of time. In all plots, we have taken the transfer time to be $t^* = 1$ and the chain consists of $N = 31$ sites.

and the energies $|E_j(t) - E_i(t)| > \epsilon_0$ are separated by a small $\epsilon_0 \, \forall t$. In the QST protocol employing the odd-sized SSH chain, initially (as $J_{odd} = 0$) the energy gap separating the zero-mode from the excited states takes its maximum value. As J_{odd} is switched-on and J_{even} decreases, the energy gap approaches its minimum, occurring at $J_{odd} = J_{even}$ and at the transfer time t^* regains its maximum value (e.g. see Fig. 5.5 (a) and (b) bottom panel). Our logic when dealing with the aforementioned dynamical evolution is simple and can be summarized into two considerations. One thing that we can do is to force the driving function to equate J_{odd} and J_{even} at values close to J_{max}, which is the maximum value the couplings can acquire during the transfer. This will result in the maximization of the minimum energy gap. The minimum energy gap can be used to specify a characteristic time scale. When the transfer time is sufficiently large compared to this time scale, we can safely assume that we are close to the adiabatic following of the zero-energy state. A driving function that has this characteristic has also been used in [103], where the dimerized chain they consider is equivalent to the SSH chain. The other crucial consideration, is to adjust the driving in such a way that, initially, when the energy gap is bigger, we "strongly" drive the system (i.e. steeper slope of the driving function) and when we are close to the minimum value of the energy gap the driving becomes more "gentle" (i.e. smaller slope). Note however here, that strongly driving the system may induce non-adiabatic transitions between the zero-energy state and the excited states, that in general reduce the efficiency of the transfer.

Recently [85], in a superconducting quibit chain that can be effectively described by an odd-sized SSH chain, an adiabatic protocol using a cosine driving function was considered. Aiming to balance the interplay between the two aforementioned consider-

ations in order to increase the speed of the transfer protocol, we propose an alternative exponential driving function. We claim that this function encapsulates the desirable crucial characteristics we considered in this section. In the next sections we will explicitly demonstrate that the proper implementation of the above leads to faster transfer process while at the same time the robustness of the protocol is maintained.

5.4 Speed of the transfer

Now let us examine in more detail the QST protocols that we briefly described in the previous section and provide the numerical evidence supporting our claims. We will examine chains of moderate length $N = 31$ sites. In the protocol we propose the couplings are driven by an exponential function (see Fig. 5.5 (b) top panel):

$$J_{odd} = (1 - e^{-\alpha t/t^*})/(1 - e^{-\alpha}) \quad \text{and} \quad J_{even} = (1 - e^{-\alpha(t^*-t))/t^*})/(1 - e^{-\alpha}) \quad (5.6)$$

where $\alpha = 6.0$ is a free parameter that has been fine-tuned to increase the efficiency in terms of speed. We will get back to the role of this free parameter at the end of the current section. The exponential protocol will be compared with the cosine protocol proposed in [85] (see Fig. 5.5 (a) top panel), in which:

$$J_{odd} = b(1 - \cos(\pi t/t^*)) \quad \text{and} \quad J_{even} = b(1 + \cos(\pi t/t^*)) \quad (5.7)$$

with a constant parameter $b = 0.5$. On the other hand, for the trivial protocol the driving function has the following linear form (see Fig. 5.5 (c) top panel):

$$J_1 = \frac{t}{t^*}, \quad J_{N-1} = 1 - \frac{t}{t^*} \quad \text{and} \quad J_i = J_{max} = 1, \forall i \neq 1, N-1 \quad (5.8)$$

In Fig. 5.5, we plot for each protocol on the top panel the driving function for the couplings and on the bottom how the instantaneous eigenspectrum evolves over time. Comparing the two protocols that employ the topological chain (see Fig. 5.5 (a) and (b)), we can immediately notice their qualitative differences. The cosine function initially for large values of the energy gap, drives the system slowly, meaning the numerator of Eq. 7.4 is smaller as compared to the exponential. However, it approaches the minimum value of the energy gap with greater slope, while the exponential slows down and drives the system more smoothly in this region. Last but not least, the minimum value of the energy gap is analytically obtained by plugging into Eq. 5.3, the instantaneous values of the couplings at $t = t^*/2$. For the cosine we get $g_{min}^{cos} = 0.09$, while for the exponential $g_{min}^{exp} = 0.18$. As it was already mentioned, this is because the exponential equates J_{even} and J_{odd} at higher values.

In the trivial protocol on the other hand (Fig. 5.5 (c)), the evolution is completely different. Namely, the instantaneous energy gap separating the zero-energy mode with the rest of the modes starts from its minimum value ($g_{min}^{triv} = 0.1$), slowly increases reaching its maximum ($g_{max}^{triv} = 0.14$) at the middle of the time evolution and then returns to its initial value.

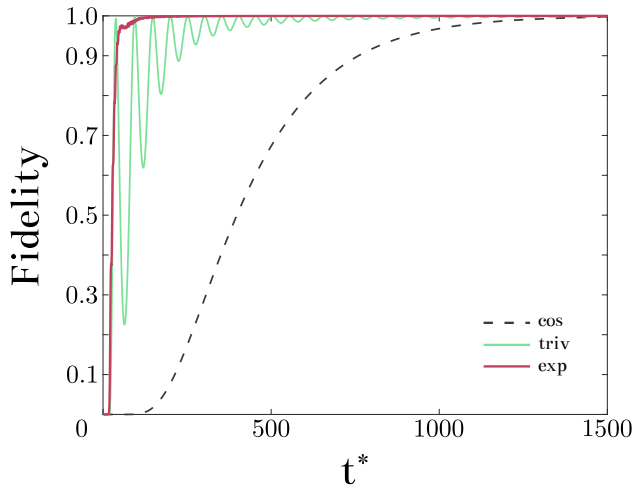

Figure 5.6: Fidelity as a function of the transfer time for all protocols.

Now, that the qualitative differences between the protocols have become apparent, let us proceed and examine some quantitative results. In Fig. 5.6, for each protocol, we plot the fidelity $\mathcal{F}$ (Eq. 5.4) as a function of the transfer time t^*. To make a comparison in terms of the speed of the transfer we have to set a lower bound in fidelity. In particular, we will consider the time after which the fidelity is stabilized above 0.9. In this case, the exponential protocol is clearly faster than the cosine protocol, since this occurs for $t^* \geq 42$ as compared to the cosine where this happens for $t^* \geq 761$. The trivial protocol on the other hand, even though it reaches $\mathcal{F} = 0.9$ for $t^* = 35$, appears to have a strongly oscillatory behavior that prevents its stabilization above $\mathcal{F} = 0.9$ till $t^* \geq 231$.

For all profiles, in the limit of $t^* \to \infty$ the fidelity approaches unity and the excitation is perfectly transferred along the chain. This makes up the adiabatic limit where, during the dynamical evolution, we "follow" the zero-energy state, without exciting other eigenstates. The oscillations that appear in the fidelity plot of the trivial protocol are in general undesirable in QST protocols since they demand great precision when tuning the transfer time [69]. Moreover, they signify that non-adiabatic processes are the underlying mechanism responsible for achieving high values of fidelity in such small transfer times. Taking a closer look at the fidelity plot of the exponential protocol (Fig. 5.7 for $\alpha = 6$), we can notice that small oscillations are also present here, i.e. the fidelity curve does not increase smoothly. This indicates that non-adiabatic processes are at work also in this case. Obtaining a suitable basis where these processes that occur during the dynamical evolution can be rigorously tracked down, remains a highly non-trivial task [81, 53]. Nevertheless, as we will now show, the non-adiabatic processes can be properly handled to increase the efficiency of the transfer process.

When we introduced the exponential driving function, we mentioned that the α parameter is fine-tuned ($\alpha = 6.0$). Smaller values of the a parameter lead to a less steep slope of the driving function and a smaller value of g_{min}^{exp} (i.e. J_{even}, J_{odd} equate at a smaller value). In this case, the non-adiabatic processes are suppressed and the fidelity smoothens out (see Fig. 5.7 $\alpha = 4$). Consequently, the protocol's speed is reduced since

high fidelity values are obtained for larger transfer times. On the contrary, increasing α above the fine-tuned value results to a stronger slope of the driving function and a greater value of g_{min}^{exp}. Therefore, the non-adiabatic processes take over for small transfer times and strong oscillations appear at the fidelity plot (see Fig. 5.7 $\alpha = 8$). This once again reduces the speed of the protocol. Thus, the value of this fine-tuned parameter $\alpha = 6$ is a trade-off, since it signifies the point up to which we strongly drive the system such that the speed is increased, but gently enough to avoid non-adiabatic effects.

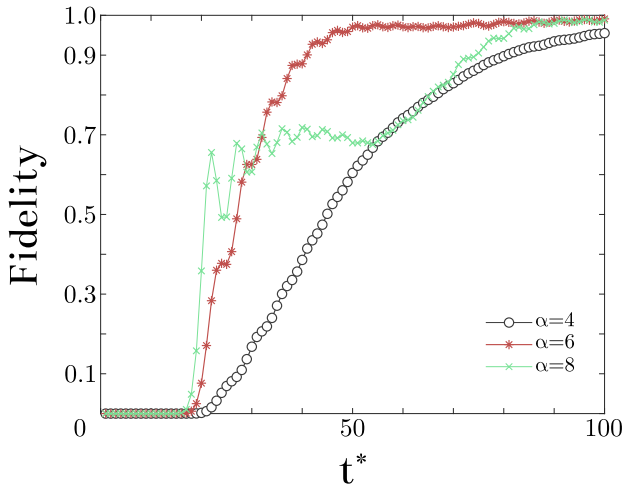

Figure 5.7: Fidelity as a function of the transfer time for the exponential driving and for different values of the α parameter.

5.5 Disorder Analysis

In this section, we will consider static disorder both on the couplings and on the magnetic field and study its effect on the transfer probability. Based on the matrix representation of the Hamiltonian the disorder on the couplings is commonly addressed to as off-diagonal disorder, while the disorder on the magnetic field as diagonal disorder. Static disorder can be attributed to manufacturing errors that arise during the experimental implementation. The way each disorder realization is imposed on the system's parameters is the following:

$$J_i(t) \to J_i(t)(1 + \delta J_i) \quad B_i(t) \to B_i(t) + \delta B_i \tag{5.9}$$

δJ_i and δB_i acquire random real values uniformly distributed in the interval $(-d_s, d_s)$, while d_s corresponds to the disorder strength. When we consider static disorder, for each realization a random profile of perturbations is imposed on the parameters and remains fixed during the time evolution.

In Fig. 5.8 for each protocol, we plot the mean transfer probability $|\langle N|N(t^*)\rangle|^2$, as a function of $\log t^*$ for diagonal and off-diagonal disorder of moderate strength $d_s = 0.2$.

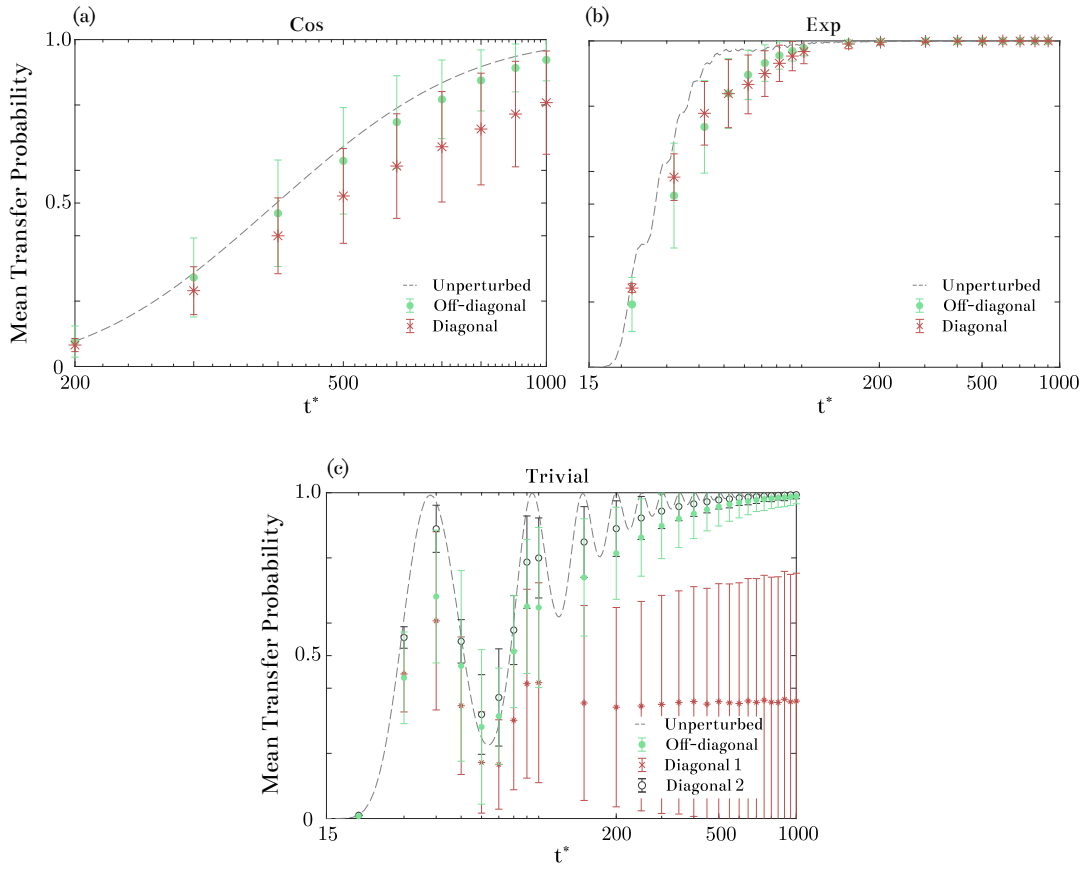

Figure 5.8: For each protocol, (a) cosine, (b) exponential and (c) trivial, we show the impact of diagonal and off-diagonal disorder of strength $d_s = 0.2$ (units of J_{max}). Each point corresponds to the mean value of the transfer probability $|\langle N|N(t^*)\rangle|^2$ averaged over 10000 disorder realizations given as a function of the transfer time, while the error bars correspond to the standard deviation of the sample. In order to compare we have also included the unperturbed curve. The transfer time axis is displayed in logarithmic scale. We also note, that the limits of the t^*-axis for the cosine differ from the other two.

We have to note here, that we use the term mean transfer probability instead of mean fidelity, to stress the fact that one should be careful and properly treat the phase γ that appears in the original definition of fidelity Eq. 2.9. In this case, since the static noise corresponds to fabrication errors, to consider the original fidelity we can assume that the phase factor γ can be suitably adjusted for each realization before taking the mean value.

What we can immediately notice, is that in almost all cases (there is one exception that will be discussed later on) the effect of disorder does not ruin completely the transfer process. Instead, the main effect is that in the presence of disorder (diagonal or off-diagonal), the transfer time t^* needed to reach high values of transfer probability is increased.

Let us turn our attention to the protocols employing the SSH chain. The zero-energy mode of the underlying static chain is known to be robust against perturbations that respect chiral symmetry [4]. Off-diagonal (chiral) disorder may change the mode's wavefunction, however its energy remains pinned down to zero. On the contrary, diagonal disorder breaks chiral symmetry and the energy of the mode is shifted. For the time-driven chain a difference between chiral and non-chiral disorder becomes apparent in the case of the adiabatic cosine protocol (see Fig. 5.8 (a)). As it was expected from the static case, the transfer probability reduces more in the presence of non-chiral disorder [85, 79]. The exponential protocol however, seems indifferent to whether the disorder is chiral or not (see Fig. 5.8 (b)). The reason behind this lies in the higher speed of the exponential protocol. Since the effect of disorder strongly manifests in large time scales, the adiabatic cosine protocol is far more sensitive compared to the exponential. This argument has been recently used to justify the resilience of the counter adiabatic protocol in [45].

When we examine the effect of the disorder on the couplings for the topologically trivial protocol (see Fig. 5.8 (c)) we observe that the oscillatory behavior of the transfer probability for small transfer times is suppressed (i.e. less oscillations and the mean transfer probability is significantly degraded). Thus, we can deduce that the resonant processes are not so robust to the static off-diagonal disorder.

On the other hand, when considering the effect of the disorder on the magnetic field we distinguish two cases. One where the disorder is imposed on all sites of the chain and another where the first and last sites are exempted (i.e. $\delta B_1 = \delta B_N = 0$). In the latter case, the protocol proves to be even more robust than the off-diagonal case (see Fig. 5.8 (c) diagonal 2). However, in the former, the effect of disorder is severe and the transfer process is completely destroyed (see Fig. 5.8 (c) diagonal 1). The diagonal disorder on the edges greatly affects the transfer process since it induces an energy difference between the initial and the final state. The system's initial state is localized on the first site with energy equal to δB_1, while the final state is localized on site N with energy δB_N. Combined with the fact that the energy gap separating them from the rest of the excited states takes its minimum value (which is smaller than the strength of the disorder) during the beginning and the end of the transfer process, explains the high impact of the diagonal disorder on the edges. In conclusion, the topological pro-

tection coming from the energy gap, clearly favors the topological channels, which are indifferent to whether the diagonal disorder is imposed on the edge sites.

To sum up, the exponential protocol is quite robust to both diagonal and off-diagonal disorder and clearly outperforms the two other protocols. As opposed to the adiabatic cosine protocol, it is indifferent to whether the disorder is chiral or not and compared with the trivial chain we can deduce that no significant (in terms of affecting the transfer probability) resonant processes susceptible to static noise are at work. Finally, the presence of a wide energy gap in the underlying static SSH chain clearly favors the topological quantum channel when the diagonal disorder is imposed on the edge sites of the chain.

5.6 Scalability

The last thing we will examine is a crucial aspect determining the efficiency of a QST protocol, commonly referred to as scalability. Meaning: how does the protocol behaves when we increase the system's size. To numerically examine this property, we pick up an arbitrary fidelity and plot the transfer time t^* it takes to reach it as a function of the system's size N. For consistency with the analysis made so far, we once again pick $\mathcal{F} = 0.9$ and examine chains up to $N = 100$ (see Fig. 5.9). We have to note, that in the case of the trivial protocol, we pick up the transfer time $t^*_{0.9}$ after which the oscillations of fidelity do not lead to a decreased fidelity value below the imposed bound (i.e. $\mathcal{F} < 0.9$). Considering the SSH protocols, as the system size is increased the value of the minimum instantaneous energy gap decreases. Consequently, to reach the desirable value of fidelity, the system has to be driven at a slower pace. Nevertheless, by inspecting Fig. 5.9, it is evident that the proposed exponential driving outperforms the two other protocols in terms of the transfer time and exhibits a good behavior up to the lengths we have considered here.

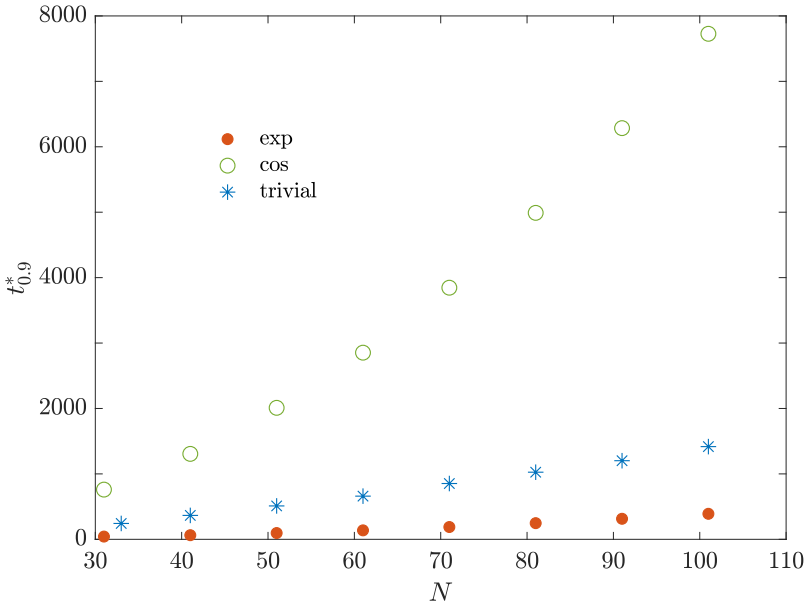

Figure 5.9: For each protocol, we plot the transfer time $t^*_{0.9}$ it takes to reach $\mathcal{F} = 0.9$ as a function of the system's size N.

Chapter 6

Conclusions and outlook

We have studied the problem of transferring states between vertices of a quantum network. In the first chapters of this work we focused on the engineered couplings protocol, while on the last chapter a time-dependent protocol was considered.

Concerning the engineered couplings protocol, by examining the conditions (reachability criteria) for the manifestation of perfect state transfer between an arbitrary pair of vertices in open and closed geometries, we identified the reachable and non-reachable transfer processes depending on the size of the chain [97]. For open chains, we highlighted the existence of non-mirror symmetric patterns that emerge in the profile of the couplings. The analytical treatment that has been previously developed to deal with the transfers between mirror symmetric vertices, proves insufficient in these cases. To this end, we developed a scheme that enables us to analytically tackle the problem. This scheme sheds light to the mathematical complexity of the problem which increases with the chains size and inevitably at some point the analytical treatment becomes infeasible. Our results are supported by the numerical implementation of an optimization algorithm from which we can extract the profile of the couplings. An interesting finding that we came up with, when examining closed geometries, is that we identified a class of networks that do not support PST between any two vertices. This class of networks consists of all odd-sized cycles apart from the $N = 3$ case.

To find the root of the underlying symmetry that dictates the couplings' profile, we turned our attention to the graph theoretical tools that have been developed to treat PST in arbitrary network configurations. Exploiting the relation between cospectrality and the recently introduced notion of Latent Symmetry, the latter is identified as "core" geometrical symmetry that two vertices should possess in order to support PST. Latent symmetry is defined in terms of the isospectral reduction, which enables us to identify non trivial automorphisms between two vertices of the graph.

We have investigated the implications of the connections between cospectrality, latent symmetry and the first criterium for PST [106]. More specifically, we highlighted the fact, that the geometrical interpretation of cospectrality succeeds in providing an intuitive picture for one of the first reachability criterium in terms of walks in the network.

We have demonstrated that performing the isospectral reduction over a pair of vertices and imposing latent symmetry, we can obtain the symmetry profile of the couplings that satisfies the first reachability criterium. This provides a consistent analytical method for deducing whether two vertices can support PST based on the geometry of the network and also gives invaluable information for the numerical treatments (optimization algorithm or inverse eigenvalue methods). Moreover, we have connected the non-mirror symmetric patterns of the couplings, that we have previously encountered, to the network's non-trivial automorphisms. In this way, we showed that the isospectral reduction proves to be a powerful tool that allows us to design networks whose geometry complies with the first reachability criterium. On the other hand, the second reachability criterium imposes restrictions on the eigenvalues and there is no apparent way (at least to our knowledge) to relate this criterium to the geometry of the network. To this end, the only resources we have at our disposal are the aforementioned numerical treatments. Lastly, we have also addressed the case where the Hamiltonian of the network possess degenerate eigenvalues and demonstrated how the notion of strong cospectrality, that has been alleged to be one of the necessary and sufficient conditions for PST, ensures that the degenerate subspace meets the condition demanded by the second reachability criterium.

For PST to occur, the two reachability criteria have to be simultaneously satisfied. The isospectral reduction can be used to exclude PST, when the geometry of the network does not comply with the symmetries that are imposed on the profile of the couplings by the first reachability criterium. However, there are cases where, eventhough the profile of the couplings respects latent symmetry, their weights cannot be suitably adjusted to enforce the second criterium on the system's eigenvalues. These cases are the most difficult to handle and the analytical treatment that was developed in the first chapter of this work makes a step towards addressing this issue. The most striking example where the two conditions fail to be simultaneously satisfied, is the family of odd weighted cycles (besides $N = 3$). This example opens the perspective of employing the machinery that has been developed so far, towards obtaining a no-go theorem for particular classes of weighted graphs were PST will be impossible between any pair of vertices.

Another potential use of the engineered couplings protocols is the generation of entangled states through the phenomenon of fractional state transfer. Extending the methodology that we introduced when studying PST, we considered reachable and non-reachable transfers in an open chain between one initial and two target sites. We showed that, the bipartite nature of the chain proves to be restrictive on the values that the relative phase of the entangled state can acquire. Based on our numerical findings, we tried to unravel the pattern of reachable transfer as the systems' size grows and we also analytically determined the reachability criteria that have to be imposed on the systems' eigenvalues and eigenvectors.

In this case, the relations are more tedious to handle and so far an geometrical interpretation in terms of network symmetries is missing. Meaning the symmetries that appear in the coupling's profile remain in general unidentified. Investigating the isospectral reduction over the three sites involved in the FST, might help to shed some light towards this direction.

In the final chapter, we have numerically investigated a time-dependent protocol that employs a topological quantum chain to act as a quantum channel for transferring single-site excitations [96]. We propose an exponential driving function that increases the efficiency of the transfer in terms of speed. To sustain our claim, we make a comparison with two other QST protocols. The crucial characteristics of the exponential function are the fact that it suitably adapts the slope of the driving function based on the value of the instantaneous energy gap, while at the same time ensures that the minimum value of the energy gap is as big as possible. In addition, we studied the effect of diagonal and off-diagonal static noise highlighting the fact that even though the speed of the protocol is increased its robustness is maintained and lastly, we numerically verified that the exponential protocol outperforms the other two protocols when we increase the system's size. The difference in terms of speed with the cosine and the trivial protocol, emphasizes the power of our treatment and identifies the considerations that have to be taken into account when driving a topological quantum chain. The developed scheme makes a substantial contribution to speeding-up adiabatic protocols (with topological characteristics or not) since it indicates a conceptual way of designing the control schemes depending on the instantaneous eigenspectrum characteristics.

To conclude, on the one hand we have considered one of the fastest time-independent protocols for short distance quantum communication and shed light to its underlying dynamics and potential use, while on the other we took steps towards optimizing the speed of one of the more robust time-dependent proposals. Our work adds up to the ongoing effort of constructing discrete networks that can efficiently transfer and manipulate quantum states. We have witnessed first hand the vast challenges that one faces when trying to gain control over a quantum system.

Περίληψη

Εισαγωγή

Μια από τις βασικότερες διεργασίες στον κλάδο της κβαντικής πληροφορίας, είναι η αξιόπιστη μεταφορά καταστάσεων μεταξύ δυο σημείων του χώρου. Επί του παρόντος, για τη πραγματοποίηση μεταφοράς μεγάλων αποστάσεων τα φωτόνια αποτελούν την βέλτιστη επιλογή. Η κβαντική κατάσταση συνήθως κωδικοποιείται στην πόλωση των φωτονίων τα οποία μπορούν να μεταφερθούν μεταξύ δύο σημείων μέσω οπτικών ινών. Παρ΄ όλα ταύτα, έχει επισημανθεί ότι η κωδικοποίηση της πληροφορίας στα φωτόνια μπορεί να αποφευχθεί όταν η μεταφορά καταστάσεων πρόκειται να πραγματοποιηθεί μεταξύ κοντινών αποστάσεων. Στον αντίποδα των φωτονίων σε αυτήν την περίπτωση, έχουν προταθεί πρωτόκολλα επικοινωνίας τα οποία χρησιμοποιούν αλυσίδες σπιν. Εναρκτήριο έναυσμα για αυτήν την ερευνητική κατεύθυνση αποτέλεσε η εργασία του **Bose** [20]. Στην εργασία αυτή οι συνδέσεις μεταξύ των γειτονικών σπιν της αλυσίδας θεωρήθηκαν σταθερές και ομογενείς. Προετοιμάζοντας το σύστημα έτσι ώστε η κατάσταση η οποία θέλουμε να μεταφέρουμε βρίσκεται στο πρώτο πλεγματικό σημείο της αλυσίδας, το σύστημα αφήνεται ελεύθερο και εξετάζεται αν υπάρχει κάποια χρονική στιγμή t^* κατά την οποία η κατάσταση έχει μεταφερθεί στο άλλο άκρο της αλυσίδας. Βασικό πλεονέκτημα του εν λόγω πρωτοκόλλου είναι το γεγονός ότι δεν απαιτείται δυναμικός έλεγχος των παραμέτρων του συστήματος κατά τη διάρκεια της μεταφοράς (χρονοανεξάρτητο πρωτόκολλο). Το μέγεθος που καθορίζει πόσο αξιόπιστα μεταφέρεται μια κατάσταση ονομάζεται πιστότητα και όταν αυτή η ποσότητα είναι ίση με 1 λέμε ότι έχουμε τέλεια μεταφορά μιας κατάστασης. Ο **Bose** μελέτησε πώς μεταβάλλεται η πιστότητα της μεταφοράς καθώς το μέγεθος της αλυσίδας μεγαλώνει. Διαπίστωσε ότι χρησιμοποιώντας το παραπάνω πρωτόκολλο ο μέγιστος αριθμός πλεγματικός αριθμός σημείων μιας αλυσίδας που δύναται να μεταφέρει τέλεια μια κατάσταση είναι $N = 4$. Αν και το αποτέλεσμα αυτό δεν ήταν ιδιαίτερα ενθαρρυντικό για την πρακτική εφαρμογή του πρωτοκόλλου, λίγο καιρό αργότερα προτάθηκε μία παραλλαγή αυτής της ιδέας που αντιμετώπισε το εν λόγω πρόβλημα. Στις μελέτες [39, 92] διαπιστώθηκε ότι η τέλεια μεταφορά μιας κατάστασης μπορεί να γίνει χωρίς την επιβολή δυναμικού ελέγχου για οσοδήποτε μεγάλες αλυσίδες, αρκεί οι συνδέσεις μεταξύ των σπιν να προκατασκευαστούν κατάλληλα. Πιο συγκεκριμένα, το προφίλ που θα πρέπει να ακολουθούν οι συνδέσεις, θα πρέπει να είναι κατοπτρικά συμμετρικό ως προς το κέντρο της αλυσίδας. Το πρωτόκολλο αυτό πετυχαίνει τη μεταφορά καταστάσεων σε μικρούς χρόνους, όμως έχει επισημανθεί

πειραματικά η δυσκολία προπαρασκευής των συνδέσεων με μεγάλη ακρίβεια καθώς και η ευαισθησία του πρωτοκόλλου στην παρουσία θορύβου. Τα προαναφερθέντα προβλήματα έχουν οδηγήσει στην μελέτη πρωτοκόλλων στα οποία οι συνδέσεις μεταξύ των σπιν ελέγχονται δυναμικά κατά την μεταφορά (χρονοεξαρτημένα πρωτόκολλα). Ιδιαίτερο ενδιαφέρον παρουσιάζουν προτάσεις οι οποίες χρησιμοποιούν σπιν αλυσίδες με τοπολογικά χαρακτηριστικά, τα οποία δύναται να προστατέψουν την διαδικασία της μεταφοράς από πηγές θορύβου και αποσυνοχής.

Τα αποτελέσματα της παρούσας μελέτης συνεισφέρουν και στις δύο προαναφερθείσες ερευνητικές κατευθύνσεις (χρονοανεξάρτητα και χρονοεξαρτώμενα πρωτόκολλα). Έναυσμα για την μελέτη μας γύρω από το χρονοανεξάρτητο πρωτόκολλο αποτέλεσε η παρατηρούμενη κατοπτρική συμμετρία των συνδέσεων στην περίπτωση της τέλειας μεταφοράς. Τα ερευνητικά ερωτήματα που διαμορφώσαμε ήταν τα εξής: Μπορεί το φαινόμενο της τέλειας μεταφοράς να συμβεί μεταξύ οποιουδήποτε αρχικού και τελικού πλεγματικού σημείου ενός κβαντικού δικτύου; Αν όχι, πότε και γιατί; Αν ναι, υπάρχει κάποια άλλη αναδυόμενη συμμετρία πέραν της κατοπτρικής; Πώς συνδέονται οι συμμετρίες στο προφίλ των συνδέσεων με την γεωμετρία του δικτύου; Επίσης, μελετήθηκε η μεταφορά μιας κατάστασης από ένα αρχικό σε δύο τελικά πλεγματικά σημεία. Η μεταφορά αυτή ονομάζεται κλασματική (fractional) και μέσω αυτής μπορεί κανείς να προετοιμάσει κβαντικά εναγκαλισμένες καταστάσεις. Όσον αφορά τα χρονοεξαρτώμενα πρωτόκολλα, επικεντρωθήκαμε στην μελέτη ενός πρωτοκόλλου που χρησιμοποιεί μια αλυσίδα με τοπολογικά χαρακτηριστικά και τα αντίστοιχα ερευνητικά ερωτήματα ήταν: Ποια είναι τα βασικά χαρακτηριστικά τα οποία πρέπει να διαθέτει η χρονοεξαρτώμενη συνάρτηση ελέγχου των συνδέσεων μεταξύ των σπιν, προκειμένου η μεταφορά να γίνεται σε μικρότερους χρόνους; Επηρεάζει η επιβολή αυτών των χαρακτηριστικών την ανθεκτικότητα του πρωτοκόλλου στην περίπτωση ύπαρξης στατικού θορύβου;

Τα αποτελέσματα της έρευνάς μας συνοψίζονται στις παρακάτω ενότητες.

Χρονοανεξάρτητο πρωτόκολλο μεταφοράς

Η Χαμιλτονιανή που χρησιμοποιείται για να περιγράψει το κβαντικό δίκτυο αναφέρεται στη βιβλιογραφία ως μοντέλο XX και έχει την κάτωθι μορφή:

$$\mathcal{H}_{XX} = \frac{1}{2} \sum_{<i,j>} J_{ij} (\hat{\sigma}_i^x \hat{\sigma}_j^x + \hat{\sigma}_i^y \hat{\sigma}_j^y) \tag{7.1}$$

Οι αλληλεπιδράσεις περιορίζονται μεταξύ πρώτων γειτόνων, θεωρούμε $\hbar = 1$, το σθένος των συνδέσεων συμβολίζεται με J και οι $\hat{\sigma}_i^x, \hat{\sigma}_i^y, \hat{\sigma}_i^z$ είναι οι πίνακες του Pauli.Οι καταστάσεις του i-οστού σπιν αναπαρίστανται από τα διανύσματα δύο συνιστωσών:

$$|1\rangle = \begin{pmatrix} 1 \\ 0 \end{pmatrix}, \quad |0\rangle = \begin{pmatrix} 0 \\ 1 \end{pmatrix} \tag{7.2}$$

Η XX-Χαμιλτονιανή μετατίθεται με τον τελεστή σ^z, οπότε ο αριθμός των σπιν με προσανατολισμό πάνω ή κάτω είναι διατηρούμενη ποσότητα. Ως εκ τούτου, για τα

πρωτόκολλα μεταφοράς που θα μελετηθούν στην παρούσα εργασία, δύναται να περιοριστούμε στον υπόχωρο της Χαμιλτονιανής όπου μόνο ένα σπιν έχει προσανατολισμό προς τα πάνω. Η Χαμιλτονιανή μιας αλυσίδας αποτελούμενη από N σπιν, σε αυτόν το υπόχωρο παίρνει την παρακάτω μορφή:

$$\mathcal{H} = J \sum_{k=1}^{N-1} (|k\rangle \langle k+1| + |k+1\rangle \langle k|) \tag{7.3}$$

Το διάνυσμα $|k\rangle$ είναι συντομογραφία της κατάστασης $|0_1...1_k...0_N\rangle$, όπου μόνο το k-οστο σπιν έχει προσανατολισμό προς τα πάνω. Η πιστότητα μια μεταφοράς F μεταξύ δύο πλεγματικών σημείων n και m ορίζεται ως:

$$F = \left| \langle m| \, e^{-i\mathcal{H}t^*} \, |n\rangle \right|^2 \tag{7.4}$$

Με t^* συμβολίζουμε την χρονική στιγμή ανάκτησης της κατάστασης από το πλεγματικό σημείο m. Όταν $F = 1$ λέμε ότι έχουμε τέλεια μεταφορά μιας κατάστασης από το n στο m. Για την μεταφορά μεταξύ των πλεγματικών σημείων 1 και N έχει αποδειχθεί ότι οι συνδέσεις J_i της αλυσίδας πρέπει να ακολουθούν ένα κατοπτρικά συμμετρικό προφίλ τέτοιο ώστε $J_n = J_{N-n}$, όπου $n = 0, 1, ..., N-1$.

Στην μελέτη μας δεν περιοριστήκαμε στην εξέταση της τέλειας μεταφοράς μεταξύ του αρχικού και του τελικού πλεγματικού σημείου της αλυσίδας, αντιθέτως εξετάστηκαν όλες τις δυνατές μεταφορές μεταξύ όλων των συνδυασμών αρχικών και τελικών σημείων του πλέγματος. Αρχικά μελετήθηκαν ανοιχτές και κλειστές αλυσίδες. Με τον όρο κλειστές αλυσίδες εννοούμε ότι το τελευταίο σπιν συνδέεται με το πρώτο, ενώ για τις ανοιχτές η σύνδεση αυτή απουσιάζει. Βασικό αριθμητικό εργαλείο στην μελέτη μας αυτή υπήρξε ένας αλγόριθμος βελτιστοποίησης. Μελετώντας αλυσίδες μεγέθους μέχρι $N = 20$ χαρτογραφήσαμε τις περιπτώσεις που η τέλεια μεταφορά είναι δυνατή και εξαγάγαμε το προφίλ των συνδέσεων J_i καθώς και την τιμή του χρόνου ανάκτησης t^*. Στις ανοιχτές αλυσίδες, αναδείξαμε την ύπαρξη μεταφορών για τις οποίες το προφίλ των συνδέσεων δεν διαθέτει κάποια εμφανή χωρική συμμετρία, ενώ παρατηρήθηκε ότι για όλες τις κλειστές γεωμετρίες μονού αριθμού πλεγματικών σημείων, εξαιρουμένης της περίπτωσης $N = 3$, δεν δύναται να καταστεί δυνατή η τέλεια μεταφορά μεταξύ οποιουδήποτε ζεύγους πλεγματικών σημείων.

Η Χαμιλτονιανή του συστήματος στο χώρο των θέσεων μπορεί να αναπαρασταθεί σε πίνακα $\mathcal{N}$, ο οποίος θα ικανοποιεί την εξίσωση ιδιοτιμών:

$$\mathcal{H}_N \, |v_i\rangle = E_i \, |v_i\rangle \tag{7.5}$$

Οι ικανές και αναγκαίες συνθήκες για την τέλεια μεταφορά εξήχθησαν αναλυτικά και συνοψίζονται στις παρακάτω δύο σχέσεις οι οποίες αφορούν τις ιδιοενέργειες και τις συνιστώσες των ιδιοδιανυσμάτων του συστήματος.

$$(E_j - E_i)t^* = \nu_{ij}\pi, \quad \nu_{ij} \in \mathbb{Z} \tag{7.6α}$$

$$\langle v_i|n\rangle = \pm \langle v_i|m\rangle \tag{7.6β}$$

Βάσει των παραπάνω σχέσεων αναπτύξαμε μια αναλυτική μεθοδολογία η οποία μας επιτρέπει να αποφανθούμε αν μια τέλεια μεταφορά μεταξύ δύο πλεγματικών σημείων

μπορεί να υποστηριχθεί από το εκάστοτε υποκείμενο χβαντικό δίκτυο. Η μεθοδολογία μας βασίζεται στην μελέτη του συστήματος εξισώσεων που προκύπτει από την εξίσωση ιδιοτιμών. Εξισώνοντας τις συνιστώσες των ιδιοδιανυσμάτων που αντιστοιχούν στα υπό εξέταση πλεγματικά σημεία εξάγονται πολυώνυμα της ενέργεια του συστήματος, οι λύσεις των οποίων πρέπει να ικανοποιούν την Εξ. 7.6α. Κατ΄ αυτόν τον τρόπο, επιβεβαιώσαμε αναλυτικά τα αριθμητικά αποτελέσματά μας για τα μεγέθη αλυσίδων που η πολυπλοκότητα ανάλυσης των πολυωνύμων επέτρεπε τον αναλυτικό χειρισμό.

Λανθάνουσα συμμετρία

Έχοντας αναδείξει την ύπαρξη μη-κατοπτρικά συμμετρικών λύσεων στο προφίλ των συνδέσεων η αναζήτηση της υποκείμενης γεωμετρικής συμμετρίας του δικτύου, έστρεψε την προσοχή μας σε μελέτες στις οποίες το φαινόμενο της τέλειας μεταφοράς είχε εξεταστεί υπό το πρίσμα της μαθηματικής θεωρίας των γράφων. Το χρονοανεξάρτητο πρωτόκολλο τέλειας μεταφοράς μπορεί να ιδωθεί ισοδύναμα ως ένας συνεχής χβαντικός περίπατος σε έναν σταθμισμένο γράφο, με την Χαμιλτονιανή να αντιστοιχεί στον πίνακα γειτνίασης του γράφου. Δύο πλεγματικά σημεία του γράφου για τα οποία ισχύει η σχέση Εξ. 7.6β ονομάζονται συνφασματικά (cospectral). Ένας εναλακτικός ορισμός της συνφασματικότητας (cospectrality) μέσω των δυνάμεων του πίνακα της Χαμιλτονιανής:

$$(H^k)_{a,a} = (H^k)_{b,b}, \quad \forall k \tag{7.7}$$

μας επιτρέπει την γεωμετρική ερμηνεία μιας εκ των δύο ικανών και αναγκαίων συνθηκών για την τέλεια μεταφορά. Πιο συγκεκριμένα, για να μπορεί να πραγματοποιηθεί τέλεια μεταφορά μεταξύ των πλεγματικών σημείων a και b θα πρέπει το άθροισμα όλων των σταθμισμένων περιπάτων k-βημάτων με αρχικό και τερματικό σημείο το a να είναι ίσο με το αντίστοιχο άθροισμα με αρχικό και τερματικό σημείο το b. Επιπρόσθετα, η ιδιότητα της συνφασματικότητας σε μία πρόσφατη μελέτη [73] συνδέθηκε με τη νεοεισαχθήσα έννοια της λανθάνουσας συμμετρίας (latent symmetry) μεταξύ δύο πλεγματικών σημείων.

Η λανθάνουσα συμμετρία μεταξύ δύο πλεγματικών σημείων ενός δικτύου αποκαλύπτεται μέσω ενός μετασχηματισμού ισοφασματικής αναγωγής του πίνακα της Χαμιλτονιανής στα εν λόγω σημεία. Η ισοφασματική αναγωγή ενός πίνακα ως προς ένα σύνολο πλεγματικών σημείων S ορίζεται ως εξής:

$$R_S(H, \lambda) = H_{SS} - H_{S\bar{S}}(H_{\bar{S}\bar{S}} - I\lambda)^{-1}H_{\bar{S}S} \tag{7.8}$$

με $\bar{S}$ να αντιστοιχεί στο συμπλήρωμα του S, δηλαδή τα υπόλοιπα πλεγματικά σημεία τα οποία δεν περιέχονται στο S. Οι πίνακες H_{SS} και $H_{\bar{S}\bar{S}}$ κατασκευάζονται διαγράφοντας από τη Χαμιλτονιανή όλα τα πλεγματικά σημεία που αντιστοιχούν στο $\bar{S}$ και S αντιστοίχως, ενώ οι $H_{S\bar{S}}$ και $H_{\bar{S}S}$ αντιστοιχούν στους πίνακες σύνδεσης μεταξύ του συνόλου S και $\bar{S}$. Στόχος της ισοφασματικής αναγωγής είναι η αναγωγή του αρχικού πίνακα σε ένα πίνακα μικρότερης διάστασης R_S (ίσης με τον αριθμό των στοιχείων του συνόλου S), ο οποίος διατηρεί το φάσμα του αρχικού. Για να γίνει

αυτό εφικτό τα στοιχεία του R_S δίνονται από ρητές συναρτήσεις της παραμέτρου λ. Μέσω της ισοφασματικής αναγωγής δύναται να αποκαλυφθούν μη τετριμμένοι αυτομορφισμοί μεταξύ των πλεγματικών σημείων της Χαμιλτονιανής. Η μελέτη μας αναδεικνύει την λανθάνουσα συμμετρία, ως την γεωμετρική συμμετρία που θα πρέπει να υπάρχει μεταξύ δύο πλεγματικών σημείων του δικτύου προκειμένου να μπορεί να μεταφερθεί τέλεια μια κατάσταση από το ένα στο άλλο. Οι λύσεις των μη-κατοπτρικών προφίλ συνδέσεων που παρατηρήθηκαν στις ανοιχτές γεωμετρίες αντιστοιχούν στους προαναφερθείσες μη-τετριμμένους αυτομορφισμούς του δικτύου. Επιπρόσθετα, χρησιμοποιώντας την ισοφασματική αναγωγή μπορούμε να εξαγάγουμε τις συμμετρίες του προφίλ των συνδέσεων και να αποφανθούμε για την δυνατότητα επίτευξης της τέλειας μεταφοράς βάσει της γεωμετρίας του δικτύου.

Τέλος μελετήθηκε η έννοια της ισχυρής συνφασματικότητας(strong cospectrality) μεταξύ δύο σημείων, η οποία συνδέθηκε αναλυτικά με τις δύο ικανές και αναγκαίες συνθήκες για την τέλεια μεταφορά κατά την παρουσία εκφυλισμένων ιδιοτιμών στο δίκτυο.

Κλασματική μεταφορά καταστάσεων

Μια ακόμη εφαρμογή του χρονοανεξάρτητου πρωτοκόλλου προπαρασκευασμένων συνδέσεων, είναι η μελέτη της κλασματικής μεταφοράς καταστάσεων με στόχο την δημιουργία εναγκαλισμένων καταστάσεων. Στο πλαίσιο αυτό μελετήσαμε την κλασματική μεταφορά μεταξύ ενός τυχαίου αρχικού (n) και δύο τυχαίων τελικών $(m,\ k)$ πλεγματικών σημείων μιας ανοιχτής αλυσίδας. Η πιστότητα της μεταφοράς σε αυτήν την περίπτωση ορίζεται ως:

$$F = \left|(\cos\chi \langle m| + e^{i\theta}\sin\chi \langle k|)e^{-iHt}|n\rangle\right|^2 \tag{7.9}$$

όπου $\chi \in (0, \pi/2)$ και $\theta \in [0, 2\pi)$. Επίσης, εξαγάγαμε αναλυτικά τις ικανές και αναγκαίες συνθήκες που θα πρέπει να ικανοποιούνται από τις συνιστώσες των ιδιοδιανυσμάτων και τις ιδιοτιμές του συστήματος έτσι ώστε η κλασματική μεταφορά να είναι τέλεια $(F = 1)$. Ενώ παράλληλα, χρησιμοποιώντας αριθμητικές μεθόδους (αλγόριθμο βελτιστοποίησης) σκιαγραφήσαμε το μοτίβο των δυνατών κλασματικών μεταφορών συναρτήσει του μεγέθους της αλυσίδας και όπου ήταν δυνατόν εντοπίσαμε τις συμμετρίες στα προφίλ των συνδέσεων. Επιπρόσθετα, αναδείξαμε το πώς η γραφοθεωρητική έννοια του 2-χρωματισμού της ανοιχτής αλυσίδας επιβάλλει περιορισμούς στις τιμές της σχετικής φάσης θ μεταξύ των όρων που εμφανίζονται στην εναγκαλισμένη κατάσταση. Συγκεκριμένα δείξαμε ότι όταν $m, k \in even$ ή $m, k \in odd$, η σχετική γωνία είναι $\theta = \nu\pi$ και όταν $m \in even$ και $k \in odd$ ή το αντίστροφο, $\theta = (2\nu + 1)\frac{\pi}{2}$, όπου $\nu \in \mathbb{Z}$.

Χρονοεξαρτώμενο πρωτόκολλο μεταφοράς

Το βασικό μοντέλο το οποίο χρησιμοποιήθηκε στην περίπτωση του χρονοεξαρτώμενου πρωτοκόλλου μεταφοράς είναι η αλυσίδα Su-Schrieffer-Heeger (SSH). Σκοπός μας στην περίπτωση αυτή είναι η μεταφορά μιας κατάστασης από το ένα άκρο της αλυσίδας στο άλλο. Η Χαμιλτονιανή του μοντέλου προκύπτει με τον διμερισμό των συνδέσεων της Εξ. 7.3 κατά τον ακόλουθο τρόπο: $J_i = J_{odd}$ για $i \in odd$ και $J_i = J_{even}$ για $i \in even$. Όταν ο συνολικός αριθμός πλεγματικών σημείων της αλυσίδας είναι μονός υπάρχει πάντοτε μια ιδιοκατάσταση του συστήματος με μηδενική ενέργεια η οποία διαχωρίζεται από τις υπόλοιπες ιδιοκαταστάσεις μέσω ενός ενεργειακού χάσματος. Ανάλογα με το εάν $J_{odd} < J_{even}$ ή $J_{odd} > J_{even}$ η κατάσταση αυτή εντοπίζεται χωρικά στο πρώτο ή στο τελευταίο πλεγματικό σημείο αντιστοίχως. Συνεπώς, αν υποθέσουμε ότι τη χρονική στιγμή $t = 0$ οι συνδέσεις είναι $J_{odd} = 0, J_{even} = 1$ και η αρχική μας κατάσταση είναι εντοπισμένη στο πρώτο πλεγματικό σημείο της αλυσίδας, αυξάνοντας σταδιακά το σθένος των συνδέσεων J_{odd} ενώ παράλληλα μειώνουμε το σθένος των J_{even}, καταλήγουμε τη χρονική στιγμή $t = t^*$ να έχουμε την αντίστροφη εικόνα $J_{odd} = 1, J_{even} = 0$. Κατ΄ αυτόν τον τρόπο επιτυγχάνεται η μεταφορά της κατάστασης από το πρώτο στο τελευταίο πλεγματικό σημείο της αλυσίδας. Η πιστότητα της μεταφοράς σε αυτήν την περίπτωση θα δίνεται από τη σχέση:

$$\mathcal{F} = |\langle N|N(t^*)\rangle|^2 \tag{7.10}$$

όπου το $|N(t)\rangle$ προσδιορίζεται λύνοντας την χρονοεξαρτώμενη εξίσωση Schrödinger. Σε μια πρόσφατη μελέτη [85], αναδείχθηκε η ανθεκτικότητα του εν λόγω πρωτοκόλλου παρουσία στατικού θορύβου. Βασική προϋπόθεση για την επίτευξη υψηλής πιστότητας στη μεταφορά, αποτελεί η αδιαβατική εξέλιξη του συστήματος. Συνεπώς, για την επίτευξη υψηλής πιστότητας η χρονική διάρκεια της μεταφοράς είναι πολύ μεγαλύτερη σε σχέση με τους αντίστοιχους χρόνους ανάκτησης του χρονοανεξάρτητου πρωτοκόλλου που μελετήσαμε στις προηγούμενες ενότητες.

Η παρουσία του ενεργειακού χάσματος στην χρονοανεξάρτητη Χαμιλτονιανή, αποτελεί βασικό χαρακτηριστικό της τοπολογικής προστασίας της ιδιοκατάστασης που αντιστοιχεί στην μηδενική ενέργεια. Το μέγεθος του ενεργειακού χάσματος του συστήματος εξαρτάται από τον λόγο μεταξύ των δύο συνδέσεων J_{odd} και J_{even}. Στην παρούσα μελέτη μας, βασιζόμενοι σε συλλογισμούς που αναπτύσσουμε σε σχέση με τους όρους που υπεισέρχονται στον ορισμό του αδιαβατικού αναλλοίωτου και με γνώμονα την μορφή της εξέλιξης του στιγμιαίου ενεργειακού φάσματος, εντοπίζουμε τα βασικά χαρακτηριστικά που θα πρέπει να επιβληθούν στις χρονοεξαρτώμενες συναρτήσεις ελέγχου των παραμέτρων $J_{odd}(t)$ και $J_{even}(t)$ προκειμένου να βελτιώσουμε τον χρόνο της μεταφοράς. Προτείνουμε μια συγκεκριμένη μορφή για τη συνάρτηση ελέγχου και αναδεικνύουμε την υπεροχή της ως προς την ταχύτητα μεταφοράς, συγκρίνοντάς την με την προυπάρχουσα πρόταση [85] και με ένα χρονοεξαρτώμενο πρωτόκολλο στο οποίο η υποκείμενη Χαμιλτονιανή της αλυσίδας δεν διαθέτει τοπολογικά χαρακτηριστικά. Επιπρόσθετα, επιβεβαιώνουμε ότι η ανθεκτικότητα του πρωτοκόλλου μένει ανεπηρέαστη υπό την παρουσία στατικού θορύβου και συγκρίνουμε τις επιπτώσεις του θορύβου μεταξύ των πρωτοκόλλων που η χρονοανεξάρτητη Χαμιλτονιανή διαθέτει τοπολογικά χαρακτηρίστηκα και του πρωτοκόλλου που η Χαμιλτονιανή είναι

τοπολογικά τετριμμένη. Ισχυριζόμαστε ότι η μέθοδός μας είναι γενική και δύναται να χρησιμοποιηθεί για την βελτιστοποίηση του χρόνου μεταφοράς καταστάσεων σε αδιαβατικά πρωτόκολλα.

Bibliography

[1] RR Agundez, Charles D Hill, Lloyd CL Hollenberg, Sven Rogge, and Miriam Blaauboer. Superadiabatic quantum state transfer in spin chains. *Physical Review A*, 95(1):012317, 2017.

[2] Jonathan Allcock and Noah Linden. Quantum communication beyond the localization length in disordered spin chains. *Physical Review Letters*, 102(11):110501, 2009.

[3] Frank Arute, Kunal Arya, Ryan Babbush, Dave Bacon, Joseph C Bardin, Rami Barends, Rupak Biswas, Sergio Boixo, Fernando GSL Brandao, David A Buell, et al. Quantum supremacy using a programmable superconducting processor. *Nature*, 574(7779):505–510, 2019.

[4] János K Asbóth, László Oroszlány, and András Pályi. A short course on topological insulators. *Lecture notes in physics*, 919:87, 2016.

[5] S Ashhab, PC De Groot, and Franco Nori. Speed limits for quantum gates in multiqubit systems. *Physical Review A*, 85(5):052327, 2012.

[6] I Sh Averbukh and NF Perelman. Fractional revivals: Universality in the long-term evolution of quantum wave packets beyond the correspondence principle dynamics. *Physics Letters A*, 139(9):449–453, 1989.

[7] David D Awschalom, Daniel Loss, and Nitin Samarth. Semiconductor spintronics and quantum computation. 2013.

[8] Rachel Bachman, Eric Fredette, Jessica Fuller, Michael Landry, Michael Opperman, Christino Tamon, and Andrew Tollefson. Perfect state transfer on quotient graphs. *arXiv preprint arXiv:1108.0339*, 2011.

[9] Vinitha Balachandran and Jiangbin Gong. Adiabatic quantum transport in a spin chain with a moving potential. *Physical Review A*, 77(1):012303, 2008.

[10] Leonardo Banchi, Enrico Compagno, and Sougato Bose. Perfect wave-packet splitting and reconstruction in a one-dimensional lattice. *Physical Review A*, 91(5):052323, 2015.

[11] Milan Bašić, Marko D Petković, and Dragan Stevanović. Perfect state transfer in integral circulant graphs. *Applied Mathematics Letters*, 22(7):1117–1121, 2009.

[12] Matthieu Bellec, Georgios M Nikolopoulos, and Stelios Tzortzakis. Faithful communication hamiltonian in photonic lattices. *Optics Letters*, 37(21):4504–4506, 2012.

[13] Jan Benhelm, Gerhard Kirchmair, Christian F Roos, and Rainer Blatt. Towards fault-tolerant quantum computing with trapped ions. *Nature Physics*, 4(6):463–466, 2008.

[14] Charles H Bennett and Gilles Brassard. Quantum cryptography: Public key distribution and coin tossing. *arXiv preprint arXiv:2003.06557*, 2020.

[15] Charles H Bennett, Gilles Brassard, Claude Crépeau, Richard Jozsa, Asher Peres, and William K Wootters. Teleporting an unknown quantum state via dual classical and einstein-podolsky-rosen channels. *Physical Review Letters*, 70(13):1895, 1993.

[16] Anna Bernasconi, Chris Godsil, and Simone Severini. Quantum networks on cubelike graphs. *Physical Review A*, 78(5):052320, 2008.

[17] Michael Berry, Irene Marzoli, and Wolfgang Schleich. Quantum carpets, carpets of light. *Physics World*, 14(6):39, 2001.

[18] P Bocchieri and A Loinger. Quantum recurrence theorem. *Physical Review*, 107(2):337, 1957.

[19] Péter Boross, János K Asbóth, Gábor Széchenyi, László Oroszlány, and András Pályi. Poor man's topological quantum gate based on the su-schrieffer-heeger model. *Physical Review B*, 100(4):045414, 2019.

[20] Sougato Bose. Quantum communication through an unmodulated spin chain. *Physical Review Letters*, 91(20):207901, 2003.

[21] Sougato Bose. Quantum communication through spin chain dynamics: an introductory overview. *Contemporary Physics*, 48(1):13–30, 2007.

[22] Martin Bruderer, Kurt Franke, S Ragg, W Belzig, and Danail Obreschkow. Exploiting boundary states of imperfect spin chains for high-fidelity state transfer. *Physical Review A*, 85(2):022312, 2012.

[23] Leonid Bunimovich and Longmei Shu. Generalized eigenvectors of isospectral transformations, spectral equivalence and reconstruction of original networks. *Linear Algebra and its Applications*, 551:104–124, 2018.

[24] Leonid Bunimovich and Benjamin Webb. Isospectral transformations. *Springer Monographs in Mathematics, Springer, New York*, 2014.

[25] Daniel Burgarth and Sougato Bose. Conclusive and arbitrarily perfect quantum-state transfer using parallel spin-chain channels. *Physical Review A*, 71(5):052315, 2005.

[26] Daniel Burgarth, Koji Maruyama, Michael Murphy, Simone Montangero, Tommaso Calarco, Franco Nori, and Martin B Plenio. Scalable quantum computation via local control of only two qubits. *Physical Review A*, 81(4):040303, 2010.

[27] Jian-Ming Cai, Zheng-Wei Zhou, and Guang-Can Guo. Decoherence effects on the quantum spin channels. *Physical Review A*, 74(2):022328, 2006.

[28] Tommaso Caneva, Michael Murphy, Tommaso Calarco, Rosario Fazio, Simone Montangero, Vittorio Giovannetti, and Giuseppe E Santoro. Optimal control at the quantum speed limit. *Physical Review Letters*, 103(24):240501, 2009.

[29] Paola Cappellaro, Chandrasekhar Ramanathan, and David G Cory. Simulations of information transport in spin chains. *Physical Review Letters*, 99(25):250506, 2007.

[30] Andrea Casaccino, Seth Lloyd, Stefano Mancini, and Simone Severini. Quantum state transfer through a qubit network with energy shifts and fluctuations. *International Journal of Quantum Information*, 7(08):1417–1427, 2009.

[31] Ada Chan, Gabriel Coutinho, Christino Tamon, Luc Vinet, and Hanmeng Zhan. Quantum fractional revival on graphs. *Discrete Applied Mathematics*, 269:86–98, 2019.

[32] Ada Chan, Gabriel Coutinho, Christino Tamon, Luc Vinet, and Hanmeng Zhan. Fractional revival and association schemes. *Discrete Mathematics*, 343(11):112018, 2020.

[33] Ada Chan, Whitney Drazen, Or Eisenberg, Mark Kempton, and Gabor Lippner. Approximate quantum fractional revival in paths and cycles. *arXiv preprint arXiv:2005.00492*, 2020.

[34] Ada Chan, Bobae Johnson, Mengzhen Liu, Malena Schmidt, Zhanghan Yin, and Hanmeng Zhan. Laplacian fractional revival on graphs. *arXiv preprint arXiv:2010.10413*, 2020.

[35] Robert J Chapman, Matteo Santandrea, Zixin Huang, Giacomo Corrielli, Andrea Crespi, Man-Hong Yung, Roberto Osellame, and Alberto Peruzzo. Experimental perfect state transfer of an entangled photonic qubit. *Nature Communications*, 7:11339, 2016.

[36] Bing Chen, Z Song, and CP Sun. Fractional revivals of the quantum state in a tight-binding chain. *Physical Review A*, 75(1):012113, 2007.

[37] Yu-Ao Chen, Sylvain Nascimbene, Monika Aidelsburger, Marcos Atala, Stefan Trotzky, and Immanuel Bloch. Controlling correlated tunneling and superexchange interactions with ac-driven optical lattices. *Physical Review Letters*, 107(21):210405, 2011.

[38] Matthias Christandl, Nilanjana Datta, Tony C Dorlas, Artur Ekert, Alastair Kay, and Andrew J Landahl. Perfect transfer of arbitrary states in quantum spin networks. *Physical Review A*, 71(3):032312, 2005.

[39] Matthias Christandl, Nilanjana Datta, Artur Ekert, and Andrew J Landahl. Perfect state transfer in quantum spin networks. *Physical Review Letters*, 92(18):187902, 2004.

[40] Matthias Christandl, Luc Vinet, and Alexei Zhedanov. Analytic next-to-nearest-neighbor x x models with perfect state transfer and fractional revival. *Physical Review A*, 96(3):032335, 2017.

[41] Richard Cleve and Harry Buhrman. Substituting quantum entanglement for communication. *Physical Review A*, 56(2):1201, 1997.

[42] Antonin Coutant, Vassos Achilleos, Olivier Richoux, Georgios Theocharis, and Vincent Pagneux. Robustness against disorder of topological corner modes and application to acoustic networks. *Phys. Rev. B*, 102:214204, 2020.

[43] Carlos M da Fonseca. On the location of the eigenvalues of jacobi matrices. *Applied Mathematics Letters*, 19(11):1168–1174, 2006.

[44] Li Dai, YP Feng, and LC Kwek. Engineering quantum cloning through maximal entanglement between boundary qubits in an open spin chain. *Journal of Physics A: Mathematical and Theoretical*, 43(3):035302, 2009.

[45] Felippo M D'Angelis, Felipe A Pinheiro, David Guéry-Odelin, Stefano Longhi, and François Impens. Fast and robust quantum state transfer in a topological su-schrieffer-heeger chain with next-to-nearest-neighbor interactions. *Physical Review Research*, 2(3):033475, 2020.

[46] Gabriele De Chiara, Davide Rossini, Simone Montangero, and Rosario Fazio. From perfect to fractal transmission in spin chains. *Physical Review A*, 72(1):012323, 2005.

[47] Sebastian Deffner and Steve Campbell. Quantum speed limits: from heisenberg's uncertainty principle to optimal quantum control. *Journal of Physics A: Mathematical and Theoretical*, 50(45):453001, 2017.

[48] David Deutsch. Quantum theory, the church–turing principle and the universal quantum computer. *Proceedings of the Royal Society of London. A. Mathematical and Physical Sciences*, 400(1818):97–117, 1985.

[49] Michel H Devoret and Robert J Schoelkopf. Superconducting circuits for quantum information: an outlook. *Science*, 339(6124):1169–1174, 2013.

[50] David P DiVincenzo. The physical implementation of quantum computation. *Fortschritte der Physik: Progress of Physics*, 48(9-11):771–783, 2000.

[51] David P DiVincenzo and Daniel Loss. Quantum computers and quantum coherence. *Journal of Magnetism and Magnetic Materials*, 200(1-3):202–218, 1999.

[52] Pedro Duarte and Maria Joana Torres. Eigenvectors of isospectral graph transformations. *Linear Algebra and its Applications*, 474:110–123, 2015.

[53] AM Dykhne. Quantum transitions in the adiabatic approximation. *Sov. Phys. JETP*, 11:411, 1960.

[54] Marta P Estarellas, Irene D'Amico, and Timothy P Spiller. Topologically protected localised states in spin chains. *Scientific Reports*, 7(1):1–10, 2017.

[55] Richard P Feynman. Simulating physics with computers. *Int. J. Theor. Phys*, 21(6/7), 1982.

[56] S Friedland and AA Melkman. On the eigenvalues of non-negative jacobi matrices. *Linear Algebra and Its Applications*, 25:239–253, 1979.

[57] Vincent X Genest, Luc Vinet, and Alexei Zhedanov. Exact fractional revival in spin chains. *Modern Physics Letters B*, 30(26):1650315, 2016.

[58] Vincent X Genest, Luc Vinet, and Alexei Zhedanov. Quantum spin chains with fractional revival. *Annals of Physics*, 371:348–367, 2016.

[59] Gian Luca Giorgi and Thomas Busch. Quantum state transfer in the presence of nonhomogeneous external potentials. *Physical Review A*, 88(6):062309, 2013.

[60] Vittorio Giovannetti and Daniel Burgarth. Improved transfer of quantum information using a local memory. *Physical Review Letters*, 96(3):030501, 2006.

[61] Chris Godsil, Stephen Kirkland, Simone Severini, and Jamie Smith. Number-theoretic nature of communication in quantum spin systems. *Physical Review Letters*, 109(5):050502, 2012.

[62] Chris Godsil and Gordon F Royle. *Algebraic graph theory*, volume 207. Springer Science & Business Media, 2013.

[63] Chris Godsil and Jamie Smith. Strongly cospectral vertices. *arXiv preprint arXiv:1709.07975*, 2017.

[64] Daniel Gottesman. An introduction to quantum error correction and fault-tolerant quantum computation. In *Quantum information science and its contributions to mathematics, Proceedings of Symposia in Applied Mathematics*, volume 68, pages 13–58, 2010.

[65] Lov K Grover. A fast quantum mechanical algorithm for database search. In *Proceedings of the twenty-eighth annual ACM symposium on Theory of computing*, pages 212–219, 1996.

[66] Bi-Hua Huang, Yi-Hao Kang, Ye-Hong Chen, Zhi-Cheng Shi, Jie Song, and Yan Xia. Quantum state transfer in spin chains via shortcuts to adiabaticity. *Physical Review A*, 97(1):012333, 2018.

[67] D Jaksch, JI Cirac, P Zoller, SL Rolston, R Côté, and MD Lukin. Fast quantum gates for neutral atoms. *Physical Review Letters*, 85(10):2208, 2000.

[68] Alastair Kay. Perfect state transfer: beyond nearest-neighbor couplings. *Physical Review A*, 73(3):032306, 2006.

[69] Alastair Kay. Perfect, efficient, state transfer and its application as a constructive tool. *International Journal of Quantum Information*, 8(04):641–676, 2010.

[70] Alastair Kay. Basics of perfect communication through quantum networks. *Physical Review A*, 84(2):022337, 2011.

[71] Alastair Kay. Tailoring spin chain dynamics for fractional revivals. *Quantum*, 1:24, 2017.

[72] Julia Kempe. Quantum random walks: an introductory overview. *Contemporary Physics*, 44(4):307–327, 2003.

[73] Mark Kempton, John Sinkovic, Dallas Smith, and Benjamin Webb. Characterizing cospectral vertices via isospectral reduction. *Linear Algebra and its Applications*, 594:226–248, 2020.

[74] David Kielpinski, Chris Monroe, and David J Wineland. Architecture for a large-scale ion-trap quantum computer. *Nature*, 417(6890):709–711, 2002.

[75] A Yu Kitaev. Unpaired majorana fermions in quantum wires. *Physics-Uspekhi*, 44(10S):131, 2001.

[76] Emanuel Knill, Raymond Laflamme, and Gerald J Milburn. A scheme for efficient quantum computation with linear optics. *Nature*, 409(6816):46–52, 2001.

[77] Kamil Korzekwa, Paweł Machnikowski, and Paweł Horodecki. Quantum-state transfer in spin chains via isolated resonance of terminal spins. *Physical Review A*, 89(6):062301, 2014.

[78] V Kostak, GM Nikolopoulos, and I Jex. Perfect state transfer in networks of arbitrary topology and coupling configuration. *Physical Review A*, 75(4):042319, 2007.

[79] Nicolai Lang and Hans Peter Büchler. Topological networks for quantum communication between distant qubits. *npj Quantum Information*, 3(1):1–10, 2017.

[80] Xuegang Li, Y Ma, J Han, Tao Chen, Y Xu, W Cai, H Wang, YP Song, Zheng-Yuan Xue, Zhang-qi Yin, et al. Perfect quantum state transfer in a superconducting qubit chain with parametrically tunable couplings. *Physical Review Applied*, 10(5):054009, 2018.

[81] R Lim and MV Berry. Superadiabatic tracking of quantum evolution. *Journal of Physics A: Mathematical and General*, 24(14):3255, 1991.

[82] Stefano Longhi. Topological pumping of edge states via adiabatic passage. *Physical Review B*, 99(15):155150, 2019.

[83] Stefano Longhi, Gian Luca Giorgi, and Roberta Zambrini. Landau–zener topological quantum state transfer. *Advanced Quantum Technologies*, 2(3-4):1800090, 2019.

[84] S Lorenzo, TJG Apollaro, A Sindona, and F Plastina. Quantum-state transfer via resonant tunneling through local-field-induced barriers. *Physical Review A*, 87(4):042313, 2013.

[85] Feng Mei, Gang Chen, Lin Tian, Shi-Liang Zhu, and Suotang Jia. Robust quantum state transfer via topological edge states in superconducting qubit chains. *Physical Review A*, 98(1):012331, 2018.

[86] Albert Messiah and Leonard Isaac Schiff. *Quantum mechanics*, volume 643. McGraw-Hill College, 1968.

[87] Gordon E Moore et al. Cramming more components onto integrated circuits, 1965.

[88] Christian V Morfonios, Maxim Pyzh, Malte Röntgen, and Peter Schmelcher. Cospectrality preserving graph modifications and eigenvector properties via walk equivalence of vertices. *Linear Algebra and its Applications*, 624:53–86, 2021.

[89] Michael Nauenberg, Carlos Stroud, and John Yeazell. The classical limit of an atom. *Scientific American*, 270(6):44–49, 1994.

[90] Chetan Nayak, Steven H Simon, Ady Stern, Michael Freedman, and Sankar Das Sarma. Non-abelian anyons and topological quantum computation. *Reviews of Modern Physics*, 80(3):1083, 2008.

[91] John A Nelder and Roger Mead. A simplex method for function minimization. *The computer journal*, 7(4):308–313, 1965.

[92] Georgios M Nikolopoulos, David Petrosyan, and P Lambropoulos. Coherent electron wavepacket propagation and entanglement in array of coupled quantum dots. *EPL (Europhysics Letters)*, 65(3):297, 2004.

[93] TE Northup and R Blatt. Quantum information transfer using photons. *Nature Photonics*, 8(5):356–363, 2014.

[94] Sangchul Oh, Lian-Ao Wu, Yun-Pil Shim, Jianjia Fei, Mark Friesen, and Xuedong Hu. Heisenberg spin bus as a robust transmission line for quantum-state transfer. *Physical Review A*, 84(2):022330, 2011.

[95] Jiannis K Pachos. Introduction to topological quantum computation. *Cambridge University Press*, 2012.

[96] NE Palaiodimopoulos, I Brouzos, FK Diakonos, and G Theocharis. Fast and robust quantum state transfer via a topological chain. *Physical Review A*, 103(5):052409, 2021.

[97] NE Palaiodimopoulos, I Brouzos, N Georgoulea, FK Diakonos, and PA Kalozoumis. Open and closed spin chains as multiprocessor wires: Optimal engineering and reachability. *Physical Review A*, 99(2):022331, 2019.

[98] Johathan Parker and CR Stroud Jr. Coherence and decay of rydberg wave packets. *Physical Review Letters*, 56(7):716, 1986.

[99] Edwin Pednault, John A Gunnels, Giacomo Nannicini, Lior Horesh, and Robert Wisnieff. Leveraging secondary storage to simulate deep 54-qubit sycamore circuits. *arXiv preprint arXiv:1910.09534*, 2019.

[100] Peter J Pemberton-Ross, Alastair Kay, and Sophie G Schirmer. Quantum control theory for state transformations: Dark states and their enlightenment. *Physical Review A*, 82(4):042322, 2010.

[101] Armando Perez-Leija, Robert Keil, Alastair Kay, Hector Moya-Cessa, Stefan Nolte, Leong-Chuan Kwek, Blas M Rodríguez-Lara, Alexander Szameit, and Demetrios N Christodoulides. Coherent quantum transport in photonic lattices. *Physical Review A*, 87(1):012309, 2013.

[102] David Petrosyan and P Lambropoulos. Coherent population transfer in a chain of tunnel coupled quantum dots. *Optics Communications*, 264(2):419–425, 2006.

[103] David Petrosyan, Georgios M Nikolopoulos, and P Lambropoulos. State transfer in static and dynamic spin chains with disorder. *Physical Review A*, 81(4):042307, 2010.

[104] John Preskill. Quantum computing and the entanglement frontier. *arXiv preprint arXiv:1203.5813*, 2012.

[105] Rebecca Ronke, Marta P Estarellas, Irene D'Amico, Timothy P Spiller, and Takayuki Miyadera. Anderson localisation in spin chains for perfect state transfer. *The European Physical Journal D*, 70(9):189, 2016.

[106] M Röntgen, NE Palaiodimopoulos, CV Morfonios, I Brouzos, M Pyzh, FK Diakonos, and P Schmelcher. Designing pretty good state transfer via isospectral reductions. *Physical Review A*, 101(4):042304, 2020.

[107] Sankar Das Sarma, Michael Freedman, and Chetan Nayak. Topological quantum computation. *Physics Today*, 59(7):32–38, 2006.

[108] Jay D Sau, Roman M Lutchyn, Sumanta Tewari, and S Das Sarma. Generic new platform for topological quantum computation using semiconductor heterostructures. *Physical Review Letters*, 104(4):040502, 2010.

[109] SG Schirmer and PJ Pemberton-Ross. Fast high-fidelity information transmission through spin-chain quantum wires. *Physical review A*, 80(3):030301, 2009.

[110] Allen J Schwenk. Almost all trees are cospectral. *New directions in the theory of graphs*, pages 275–307, 1973.

[111] Tao Shi, Ying Li, Zhi Song, and Chang-Pu Sun. Quantum-state transfer via the ferromagnetic chain in a spatially modulated field. *Physical Review A*, 71(3):032309, 2005.

[112] Peter W Shor. Polynomial-time algorithms for prime factorization and discrete logarithms on a quantum computer. *SIAM review*, 41(2):303–332, 1999.

[113] Dallas Smith and Benjamin Webb. Hidden symmetries in real and theoretical networks. *Physica A: Statistical Mechanics and its Applications*, 514:855–867, 2019.

[114] Senmao Tan, Raditya Weda Bomantara, and Jiangbin Gong. High-fidelity and long-distance entangled-state transfer with floquet topological edge modes. *Physical Review A*, 102(2):022608, 2020.

[115] Tian Tian, Shaochun Lin, Liang Zhang, Peiran Yin, Pu Huang, Changkui Duan, Liang Jiang, and Jiangfeng Du. Perfect coherent transfer in an on-chip reconfigurable nanoelectromechanical network. *Physical Review B*, 101(17):174303, 2020.

[116] Dimitris I Tsomokos, Sahel Ashhab, and Franco Nori. Using superconducting qubit circuits to engineer exotic lattice systems. *Physical Review A*, 82(5):052311, 2010.

[117] Pierre Van Moerbeke. The spectrum of jacobi matrices. *Inventiones mathematicae*, 37(1):45–81, 1976.

[118] Luc Vinet and Alexei Zhedanov. How to construct spin chains with perfect state transfer. *Physical Review A*, 85(1):012323, 2012.

[119] Marc JJ Vrakking, DM Villeneuve, and Albert Stolow. Observation of fractional revivals of a molecular wave packet. *Physical Review A*, 54(1):R37, 1996.

[120] Yaoxiong Wang, Feng Shuang, and Herschel Rabitz. All possible coupling schemes in xy spin chains for perfect state transfer. *Physical Review A*, 84(1):012307, 2011.

[121] David S Weiss and Mark Saffman. Quantum computing with neutral atoms. *Physics Today*, 70(7), 2017.

[122] Antoni Wójcik, Tomasz Łuczak, Paweł Kurzyński, Andrzej Grudka, Tomasz Gdala, and Małgorzata Bednarska. Unmodulated spin chains as universal quantum wires. *Physical Review A*, 72(3):034303, 2005.

[123] William K Wootters and Wojciech H Zurek. A single quantum cannot be cloned. *Nature*, 299(5886):802–803, 1982.

[124] Norman Ying Yao, Liang Jiang, Alexey Vyacheslavovich Gorshkov, Z-X Gong, Alex Zhai, L-M Duan, and Mikhail D Lukin. Robust quantum state transfer in random unpolarized spin chains. *Physical Review Letters*, 106(4):040505, 2011.

[125] John A Yeazell and CR Stroud Jr. Observation of spatially localized atomic electron wave packets. *Physical Review Letters*, 60(15):1494, 1988.

[126] Man-Hong Yung. Quantum speed limit for perfect state transfer in one dimension. *Physical Review A*, 74(3):030303, 2006.

[127] Jingfu Zhang, Gui Lu Long, Wei Zhang, Zhiwei Deng, Wenzhang Liu, and Zhiheng Lu. Simulation of heisenberg x y interactions and realization of a perfect state transfer in spin chains using liquid nuclear magnetic resonance. *Physical Review A*, 72(1):012331, 2005.

[128] Xiao-Ming Zhang, Zi-Wei Cui, Xin Wang, and Man-Hong Yung. Automatic spin-chain learning to explore the quantum speed limit. *Physical Review A*, 97(5):052333, 2018.